Spring 5-12-2017

FACILE SYNTHESIS AND CHARACTERIZATION OF GRAPHENE NANORIBBONS/POLYPYRROLE NANOCOMPOSITE

JOHARA A. AL DREAM
Pittsburg State University, kas8000262@gmail.com

FACILE SYNTHESIS AND CHARACTERIZATION OF GRAPHENE NANORIBBONS/POLYPYRROLE NANOCOMPOSITE

A Thesis Submitted to the Graduate School
in Partial Fulfillment of the Requirements
for the Degree of
Master of Science

Johara Al Dream

Pittsburg State University

Pittsburg, Kansas

May, 2017

FACILE SYNTHESIS AND CHARACTERIZATION OF GRAPHENE NANORIBBONS/POLYPYRROLE NANOCOMPOSITE

Johara Al Dream

APPROVED:

Thesis Advisor _____
Dr. Ram Gupta, Department of Chemistry

Committee Member _____
Dr. Khamis Siam, Department of Chemistry

Committee Member _____
Dr. Pawan Kahol, Department of Physics

Committee Member _____
Dr. John Franklin, Department of English and Modern Languages

ACKNOWLEDGEMENTS

First of all, I would like to thank Dr. Gupta, who is my advisor. He helped and motivated me to achieve my goals. He also helped me to improve my skills and guided me to correct my mistakes throughout the course.

The King Abdullah Scholarship helped me to complete my studies in the United States of America. I would like to thank the King Abdullah Scholarship as well.

I would like to thank my parents and other family members. My family supported me; although my father has died, I feel that he can see what I do. If my father were with me, he would be very proud of me.

I would like to thank my committee members at Pittsburg State University, Dr. Khamis Siam, Dr. Pawan Kahol, and Dr. John Franklin, for their advice and help to correct the mistakes in my thesis. I would also like to thank Pittsburg State University for the excellent services in laboratories, online services, materials and other equipment. I would like to thank Dr.Sanjay Mishra at Memphis University for recording SEM and Raman spectra of my samples.

Finally, I would like to thank my husband and my daughter. I especially thank my husband for supporting me during my studies.

FACILE SYNTHESIS AND CHARACTERIZATION OF GRAPHENE NANORIBBONS/POLYPYRROLE NANOCOMPOSITE

An Abstract of the Thesis by
Johara Al Dream

Carbon is present in various forms such as coal, carbon nanotubes, graphene, diamonds, etc. Among various forms, carbon nanotubes and graphene have attracted considerable research attention due to their high thermal stability, high mechanical strength and electrical conduction. These properties largely depend on synthesis procedure. In this work, we synthesized graphene nanoribbons using carbon nanotubes for nanocomposites with polypyrrole. Chemical oxidation was used to unzip the carbon nanotubes. These graphene nanoribbons were used to fabricate nanocomposites with polypyrrole for energy storage applications. The synthesized nanocomposites were structurally and electrochemically characterized.

The structural characterization was performed using X-ray diffraction, FT-IR, SEM, Raman, TGA, and BET surface area measurements. The electrochemical characterizations of these nanocomposites was carried out using cyclic voltammetry. The electrochemical properties were further analyzed using galvanostatic charge-discharge measurements. The specific capacitance of nanocomposites was observed to decrease with increasing scan rates and current densities. The electrochemical measurements showed the highest specific capacitance of 2,066 F/g for 3PPyGO, which was observed to decrease with increasing scan rates.

TABLE OF CONTENTS

CHAPTER PAGE
INTRODUCTION 1
1.1. Discovery of conducting polymers 2
1.2. Carbon nanomaterials 7
1.3. Objective of this work 15
EXPERIMENTAL DETAILS 17
2.1. Synthesis of unzipped graphene oxide 17
2.2. Synthesis of conducting polypyrrole 17
2.3. Synthesis of nanocomposites 18
2.4. Characterizations 18
2.4.1. Scanning electron microscopy (SEM) 18
2.4.2. X-ray diffraction (XRD) 20
2.4.3. Raman spectroscopy 20
2.4.4. Fourier transform infrared spectroscopy (FTIR) 21
2.4.5. Surface area and pore size distribution measurement technique 22
2.4.6. Thermogravimetric analysis (TGA) 23
2.4.7. Electrochemical measurements 24
RESULTS AND DISCUSSION 26
3.1. Scanning electron microscopic analysis 26
3.2. X-ray diffraction analysis 29
3.3. Raman spectroscopy 34
3.4. Fourier transform infrared spectroscopy 37
3.5. Surface area and pore size distribution measurement technique 41
3.6. Electrochemical characterizations 49
CONCLUSION 64
REFERENCES 66

LIST OF TABLES

TABLE PAGE

Table 3.1: Comparison of GO, PPy and PPyGO nanocomosites in specific capacitance as a function of scan rate 55

Table 3.2: Comparison of GO, PPy and PPyGO nanocomosites in specific capacitance as a function of current density..... 63

LIST OF FIGURES

FIGURE PAGE

Figure 1.1: Conductivity of conductive polymers compared to other materials 2
Figure 1. 2: Molecular orbitals in a diatomic molecule 4
Figure 1. 3: Energy band diagram demonstrating band gaps 5
Figure 1. 4: Chemical structure of some CPs 5
Figure 1. 5: Structures of 0D, 1D, and 2D. 8
Figure 1. 6: Russian doll model and parchment carbon nanotubes 9
Figure 1. 7: Structure of graphene nanoribbons 13
Figure 1. 8: Representation of unzipping of one wall of CNT to form a GNR 14

Figure 2.1: Geometry of SEM 19
Figure 2.2: Schematic diagram of an X-ray diffractometer 20
Figure 2.3: Geometry of FTIR 22
Figure 2.4: Diagram of BET 23
Figure 2.5: Diagram of TGA instrument 24
Figure 2.6 Schematic of three cell electrochemical measurement system 25

Figure 3.1: SEM images of GO at various magnifications 27
Figure 3.2: SEM images of PPy at various magnifications. 27
Figure 3.3: SEM images of 0.5PPyGO at various magnifications. 28
Figure 3.4: SEM images of 1.5PPyGO at various magnifications. 28
Figure 3.5: SEM images of 3PPyGO at various magnifications. 39
Figure 3.6**:** XRD of CNT 30
Figure 3.7**:** XRD of graphene nanoribbons 30
Figure 3.8**:** XRD of polypyrrole 31
Figure 3.9**:** XRD of 0.5PPyGO 32
Figure 3.10: XRD of 1.5PPyGO 33
Figure 3.11: XRD of 3PPyGO 33
Figure 3.12: Raman spectrum of GO 34

Figure 3.13: Raman spectrum of PPy.....35
Figure 3.14: Raman spectrum of 0.5PPyGO.....36
Figure 3.15: Raman spectrum of 1.5PPyGO.....36
Figure 3.16: Raman spectrum of 3PPyGO.....37
Figure 3.17: FTIR of graphene nanoribbons.....38
Figure 3.18: FTIR of polypyrrole.....39
Figure 3.19: FTIR of 0.5PPyGO.....40
Figure 3.20: FTIR of 1.5PPyGO.....40
Figure 3.21: FTIR of 3PPyGO.....41
Figure 3.22: (a) Pore size distribution and (b) Nitrogen adsorption/desorption isotherm of the GO.....42
Figure 3.23: (a) Pore size distribution and (b) Nitrogen adsorption/desorption isotherm of the PPy.....43
Figure 3.24: (a) Pore size distribution and (b) Nitrogen adsorption/desorption isotherm of the 0.5PPyGO.....44
Figure 3.25: (a) Pore size distribution and (b) Nitrogen adsorption/desorption isotherm of the 1.5PPyGO.....44
Figure 3.26: (a) Pore size distribution and (b) Nitrogen adsorption/desorption isotherm of the 3PPyGO.....45
Figure 3.27: TGA of graphene nanoribbons.....46
Figure 3.28: TGA of PPy.....46
Figure 3.29: TGA of 0.5PPyGO.....47
Figure 3.30: TGA of 1.5PPyGO.....48
Figure 3.31: TGA of 3PPyGO.....48
Figure 3.32: Cyclic voltammograms of GO sample at various scan rates in 3 M KOH electrolyte.....50
Figure 3.33: Cyclic voltammograms of PPy sample at various scan rates in 3 M KOH electrolyte.....51
Figure 3.34: Cyclic voltammograms of 0.5PPyGO sample at various scan rates in 3 M KOH electrolyte.....51

Figure 3.35: Cyclic voltammograms of 1.5PPyGO sample at various scan rates in 3 M KOH electrolyte. 52
Figure 3.36: Cyclic voltammograms of 3PPyGO sample at various scan rates in 3 M KOH electrolyte. 52
Figure 3.37: Specific capacitance as a function of scan rate for GO sample in 3 M KOH electrolyte. 53
Figure 3.38: Specific capacitance as a function of scan rate for PPy sample in 3 M KOH electrolyte. 53
Figure 3.39: Specific capacitance as a function of scan rate for 0.5PPyGO sample in 3 M KOH electrolyte. 54
Figure 3.40: Specific capacitance as a function of scan rate for 1.5PPyGO sample in 3 M KOH electrolyte. 54
Figure 3.41: Specific capacitance as a function of scan rate for 3PPyGO sample in 3 M KOH electrolyte. 55
Figure 3.42: Galvanostatic charge-discharge characteristics of GO electrode at various applied currents in 3M KOH electrolyte 57
Figure 3.43: Galvanostatic charge-discharge characteristics of PPy electrode at various applied currents in 3M KOH electrolyte. 58
Figure 3.44: Galvanostatic charge-discharge characteristics of 0.5PPy electrode at various applied currents in 3M KOH electrolyte. 58
Figure 3.45: Galvanostatic charge-discharge characteristics of 1.5PPyGO electrode at various applied currents in 3M KOH electrolyte. 59
Figure 3.46: Galvanostatic charge-discharge characteristics of 3PPyGO electrode at various applied currents in 3M KOH electrolyte. 59
Figure 3.47: Comparision of GO, PPy and 3PPPyGO in Galvanostatic charge-discharge performance. 60
Figure 3.48: Specific capacitance as a function of scan rate for GO sample in 3 M KOH electrolyte. 60
Figure 3.49: Specific capacitance as a function of current density for PPy sample in 3 M KOH electrolyte. 61

Figure 3.50: Specific capacitance as a function of current density for 0.5PPyGO sample in 3 M KOH electrolyte. 61
Figure 3.51: Specific capacitance as a function of current density for 1.5PPyGO sample in 3 M KOH electrolyte. 62
Figure 3.52: Specific capacitance as a function of current density for 3PPyGO sample in 3 M KOH electrolyte. 62
Figure 3.53: Comparison of GO, PPy and 3PPyGO in specific capacitance as a function of current density 63

CHAPTER I

INTRODUCTION

In recent decades, the fast growth of the worldwide economy, constant diminution of fossil fuels, and increased pollution in the environment has led to an ever-increasing demand of clean energy sources. For the storage and conversion of electrochemical energy, supercapacitors are a preferable choice because of their high-power capacity, low cost, environmental friendliness, and long cycle life. One of the extremely suitable materials for supercapacitor is graphene. It possesses useful characteristics such as being light in weight while having high electrical conductivity, exceptional mechanical strength and large surface area. Other materials, such as conducting polymers (CP), are also promising candidates for supercapacitors because of their low cost, greater capacity to store charges and facile synthesis. Unfortunately, conducting polymers suffer from instability and, therefore, their life cycle is limited. The working potential range of the CP electrode is limited by degradation due to oxidation during long term charge-discharge processes and, as a consequence, gradually reducing their conducting properties. In this condition, combining conducting polymers with the carbon material could be a suitable plan and method to gain an ideal capacitive characteristic, and that is what will be discussed in this project.

1.1. Discovery of conducting polymers

Most of the polymers are insulators in nature as they do not conduct electricity. These polymers are used for the coating of electric wires to ensure protection from electric shock. Scientists such as Alan Heeger, Hideki Shirakawa, and Alan MacDiarmid synthesized a conducting polymer called polyacetylene which was conductive like a metal [1]. This was synthesized in 1974 using a Ziegler-Natta catalyst. Inherent polyacetylene, which is insulating in nature, was made more conductive through oxidation using chlorine, iodine vapor, or bromine. The conductivity of doped polyacetylene was about 10^5 Sm^{-1}. The presence of conjugation in polyacetylene is responsible for conductivity. Figure 1.1 compares the electrical properties of insulators, semiconductors and metals.

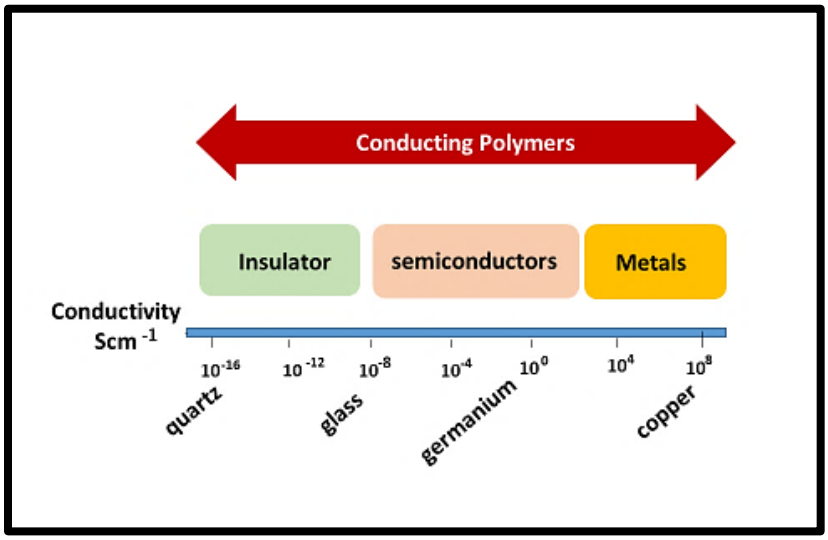

Figure 1.1: Conductivity of conductive polymers compared to other materials, from quartz (insulator) to copper (conductor).

1.1.1. Electrical conductivity

Ohm's Law defined conductivity as follows:

$$\mathbf{V = R\ I} \qquad \ldots\ldots\ldots(1)$$

Where **I** stands for the current passing through a resistor (in Amperes), **V** stands for the applied potential across it (in Volts), and **R** stands for the resistance of the sample. The unit of resistance is Ohm (Ω). For measuring the value of R, a known voltage is applied across the resistor, and the current passing through is measured.

1.1.2. The band theory

In order to have a better understanding of the conduction phenomenon in polymers, it is appropriate to have a brief discussion about the basic principles of the band theory of solids. When molecular orbital theory is related to band theory, it forms the chemical approach. The hydrogen atoms are used in the molecular orbital theory as an example (Figure 1.2). The bonding molecular orbital has a lower level of energy as compared to $H_{(1)}$ and $H_{(2)}$, as a result of delocalization of both atoms; on the other hand, the antibonding molecular orbital has a high level of energy. So, the valence band is the energy band resulting from the binding orbitals of a molecule, whereas the antibonding orbitals of the molecules result in the conduction band. Hence, the band gap is the result of differences between the highest filled energy levels and lowest filled energy levels. This band gap is denoted by E_g. (Figure 1.3). The molecular arrangement of CPs needs to be conjugated to allow the formation of delocalized electron states [2]. The nature of CP, whether it is an insulator, semiconductor, or metal, is determined by the value of the energy band gap [3].

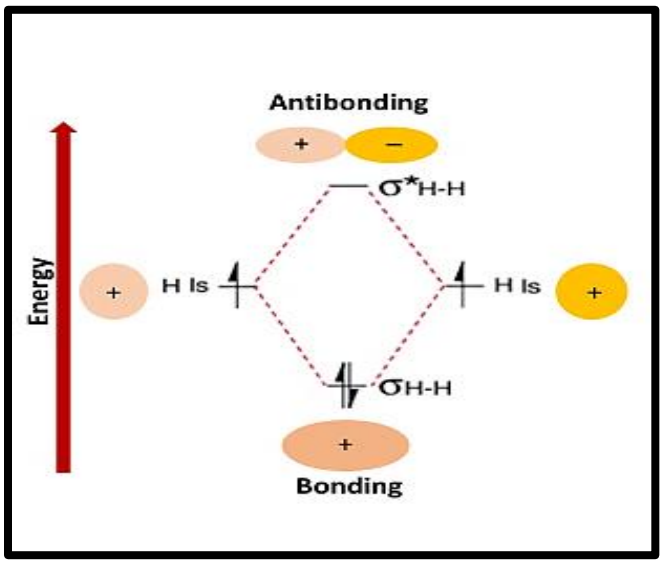

Figure 1.2: Molecular orbitals in a diatomic molecule.

1.1.3. Metals, semiconductors and insulators

The band gap of a metal is zero, because of an overlapping in the valence band and the conduction band. The band gap of insulators is higher than 3 eV [4]. Because of a larger gap between conducting band (CB) and valence band (VB), the electrons can not jump to CB under normal conditions (Figure 1.3).

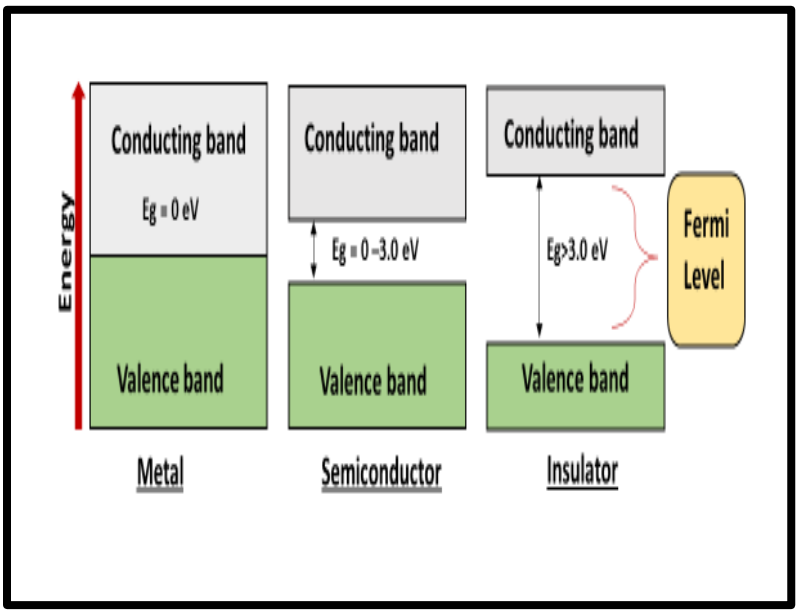

Figure 1.3: Energy band diagram demonstrating band gaps.

1.1.4. Conducting Polymers

Figure 1.4. below shows the chemical structure of some commonly used conducting polymers.

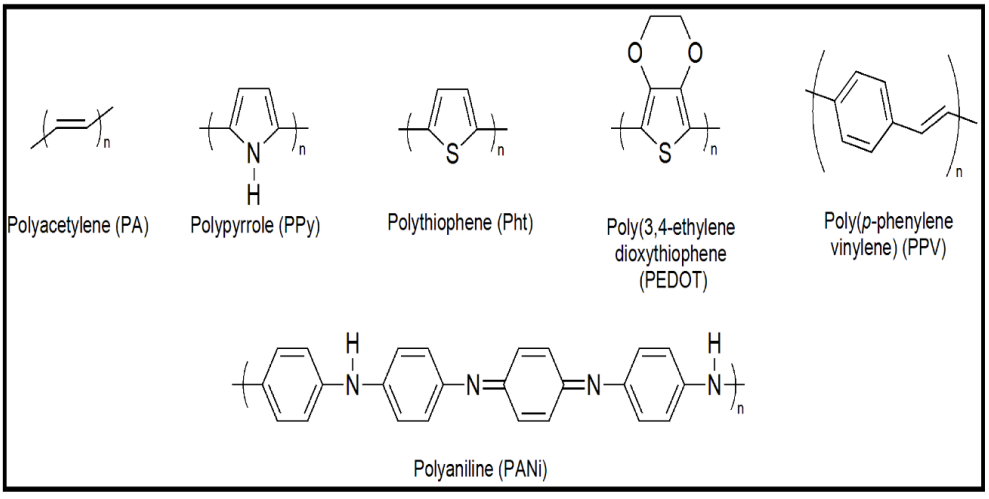

Figure 1.4: Chemical structure of some CPs (adopted from Polymers 5, 2013, 1115).

1.1.4.1. Polypyrrole (PPy)

The most significant p-type CP is polypyrrole. Polypyrrole has been used for energy storage applications because of its fast charge-discharge mechanism, high conductivity, high energy density and low cost [5-6]. It is also used in gas sensors [7], wires [8], and polymeric batteries [9]. Polypyrrole is also used in making composites with carbon-based materials [10].

1.1.4.2. Polyaniline (PANI)

Polyaniline was discovered in 1834 [11] and was analyzed in 1862 by Letheby [12]. Polyaniline is generally present in mixed oxidation states as quinoid and benzoid units [13]. This interesting feature of polyaniline was discovered by Woodhand and Green in 1912 [14]. PANI is present in various forms, including fully oxidized pernigraniline, fully reduced leucoemeraldine, and half oxidized emeraldine base. Extensive research has been conducted on PANI because of its several advantages such as high environmental stability, ease of synthesis, and high redox activities.

1.1.4.3. Polythiophenes (PTh)

The polythiophenes can be synthesized as both n and p-type. As compared to PANI and PPy, the energy storage capacity of PTh based electrode is low [15]. The derivatives of PTh, such as poly (3-(4-fluorophenyl) thiophene), (poly 3,4-ethylenedioxythiophene), and poly (3-methyl thiophene), have been used for energy storage applications. Among these derivatives, poly (3,4-ethylenedioxythiophene) (PEDOT) is considered the best material for supercapacitor applications. PEDOT/poly (styrene sulfonic acid) (PSS) is the most successful aqueous suspension, which has a high conductivity of ~ 10 S/cm [16].

Vapor phase polymerization (VPP) and liquid phase polymerization (LPP) is used to synthesize the highly conductive PEDOT.

1.2. Carbon nanomaterials

The foundation of organic chemistry relies on the fact that carbon has the capability to create different complex network arrangements. The carbon itself exhibits quite unique chemical bonds, because it exists in different allotropic forms. Diamond and graphite are the purest materials, depicting the existence of carbon in its original forms. Diamond is very hard and conducts no electricity, while graphite has a weak physical structure and is a good conductor of electricity. Many fields of science, like biology, physics, materials and especially chemistry, are now focused on the detailed study of the latest allotropic forms of carbon including nanotubes and fullerenes. The physical existence of graphene in the form of 2-D structures has been vital in the formation of further complex carbon materials having complex orientations and dimensions. Based on dimensional existence, fullerene can be supposed as the zero-dimensional compound of carbon while the nanotubes and graphite are attributed as single and three dimensional structures respectively as seen in Figure 1.5.

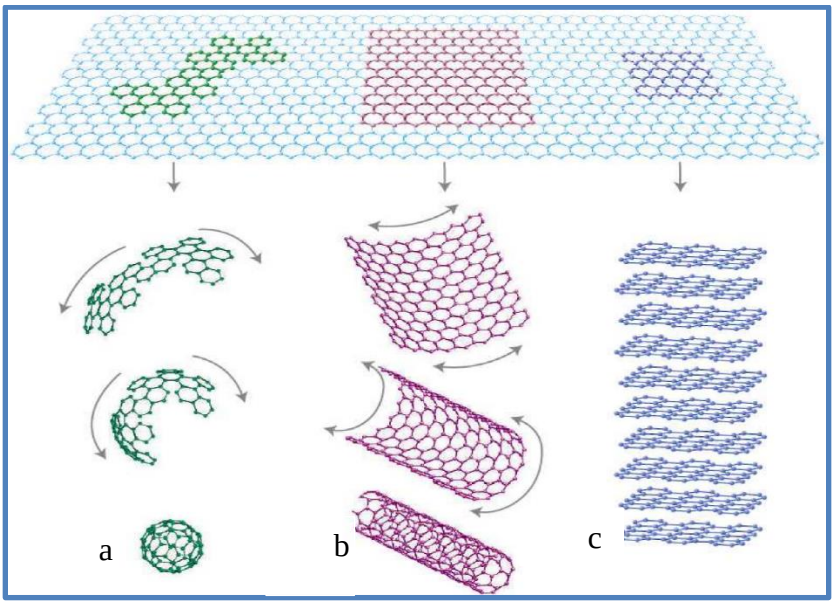

Figure 1.5: Structures of (a) 0D buck balls,(b) 1D nanotubes, and (c) 2D graphene (Adopted with permission, Nature Materials 6, 2007, 183).

1.2.1 Types of nanotubes

Carbon nanotubes are commonly found in two different forms:

1.2.1.1 Multi-walled nanotubes

Multi-walled carbon nanotubes are the first form of carbon that exists in the form of a cylinder-shaped shell formed by graphene layers. The spacing between the layers is about 3.4 nm. The multi-walled nanotubes can be characterized into two different forms. The Russian doll model consists of two tubes, an inner and outer tube, where the inner one is smaller in diameter than the outer. The second model, which is formed by rolling the single graphene sheets in multiple turns, like a piece of paper, is referred to as the Parchment model (Figure 1.6).

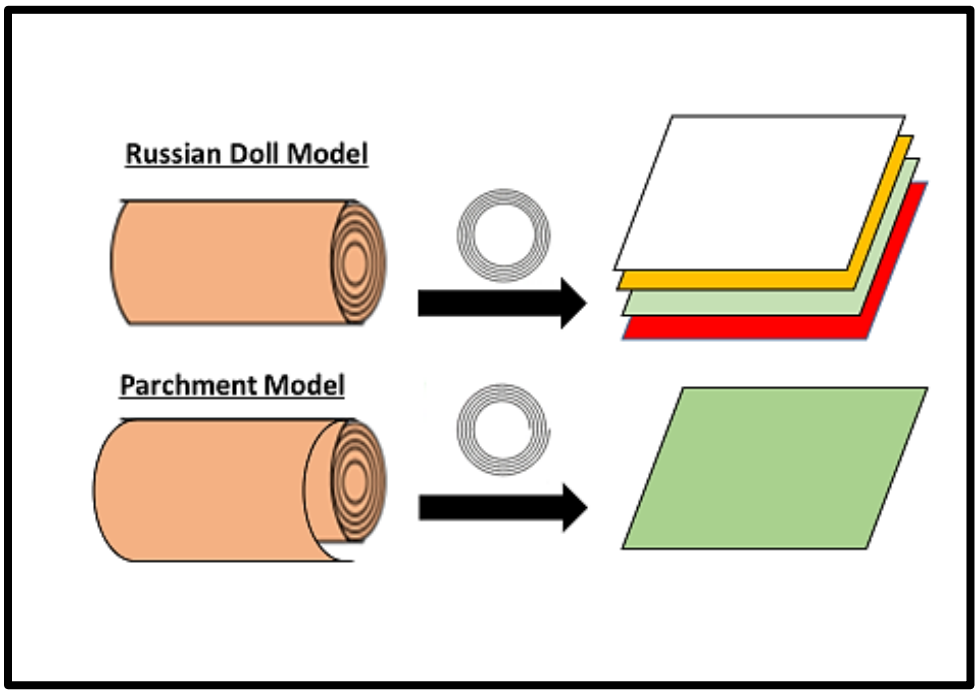

Figure 1.6: Russian doll model and parchment carbon nanotubes.

1.2.1.2 Single-walled nanotubes

Single-walled nanotubes, as one might expect, contain a single layer of the graphene sheets forming a cylinder. This type of nanotube has few benefits, such as allowing light and electromagnetic waves to pass through it easily and depicting original single dimensional behavior. Also, there are three different physical orientations in which the carbon nanotubes can be synthesized, which include Armchair, Chiral and Zigzag. Each configuration is dependent on the method by which the graphene layers have been rolled into a cylindrical structure.

1.2.2. Graphene

The graphene structure is considered to be the mother of all different kinds of carbon-bonded structures. It can be found everywhere, like in our lead pencils, which contain piles of different graphene layers stacked upon each other. Nanotubes are also

made using graphene sheets that are rolled-up, while the football-shaped molecules of fullerenes are spherically wrapped up graphene. All these different forms of graphene have been utilized in many different applications. However, their electrical, magnetic properties and elastic behavior have recently captured the attention of researchers. Graphene is one of the structural forms of carbon compounds, consisting of a single layer of carbon atoms that are packed in the form of hexagonal crystals. The length of the bond between the adjacent carbon atoms is about 0.142 nm. This material was first discovered by Geim's group which made many improvisations in the productions process later on [17]. Instead of using tape for getting these layers, the other method used by the group included the rubbing of graphite rocks along a solid surface to get fine layers. This method was also used by Phillip Kim to obtain the layers of carbon atoms [18]. Although this material has been found quite recently, because of its unique and exquisite honeycomb-like molecular arrangement, this material has attracted considerable attention towards itself.

Graphene has been the center of focused research for many years, because its unique physical properties make it transparent but highly conductive. The band-gap among different bands of carbon atoms and their electrons is responsible for the transparency. The transparency and conductivity don't exist in the same material at the same time like in indium tin oxide (ITO). Another important aspect of this material is its capacity to withstand high external stress and pressures while exhibiting structural flexibility. These characteristics have made it very suitable for electronic applications like touch screens of mobile devices [19]. The synthesis of graphene with the desired physical characteristics is based on a variety of preparation methods.

1.2.2.1 Exfoliation through scotch tape

This is a micromechanical method in which adhesive tape is used to get a layer of graphene sheets from the graphite rocks. Then, the tape is peeled off several times to reduce the multiple layers of graphene into a few numbered layers. Next, the adhesiveness of the tape is removed by putting it on a substrate covered in an acetone solution to separate the tape from the layer. The physical dimensions (like shapes and sizes) are quite varied and the thickness of the layers can range from a few nanometers to hundreds of micro-meters. The major drawback of this method is that large quantities of graphene cannot be obtained and there are also a few uncontrollable parameters. However, the major advantages with this technique are that it is not very complex or difficult to perform and the quality of the graphene layers is also quite good.

1.2.2.2. Dispersion of graphite

One method for the synthesis of a large quantity of graphene is exfoliation of graphite in liquid phase. In this way the loss of energy, in removing the layer of graphene from the crystal, is reduced. Single sheets of graphene are separated from multi-layered graphene using a centrifuge. The benefits of this process are huge scale preparation of the graphene and low complexity.

1.2.2.3. Thermal chemical vapor deposition (CVD)

Chemical vapor deposition has emerged as an effective approach for the synthesis of graphene flakes. Among other popular methods of graphene production, chemical vapor deposition appears to be a more efficient technique that is being used to produce single- or few-layer graphene films on a huge scale [20-21]. The CVD process was first used in 2006

by Somani, which produced few-layer sheets of graphene from camphor as a substrate on Ni foils [22].

1.2.2.4. Thermal deposition on silicon carbide (SiC)

The production of graphite through the scratching of the surface of silicon carbide surface in an ultrahigh vacuum has also been used in the industry to synthesize graphene. Semiconductor manufacturers are the prime users of this technique because the final product is obtained on the SiC surface, which does not need any further modification after production [23]. At high temperatures, in the presence of ultra-high vacuum, silicon atoms turn into the gaseous state, while only the carbon atoms that are left behind on the surface arrange themselves in the form of layers called graphene layers. The thickness of the layers varies and is related to time spent annealing and temperature used for heating.

1.2.3. Graphene nanoribbons (GNR)

Graphene nanoribbons are one-dimensional structures of graphene typically obtained through unzipping the carbon nanotubes. Their magnetic and electronic properties have been studied and experimented on extensively. Their electronic properties have a diverse range, including normal semiconductors to spin polarized half metals, and they have the potential of opening GNRs as electric devices. The nonchiral GNR is divided into two categories depending on the termination style, and it includes zigzag and armchair. Zigzag GNR is classified by the zigzagging chains, whereas, dimmer lines across the ribbon present the structure of armchair (Figure 1.7). The geometric structures are repeated by GNRs perpendicular to the defined width. The edge atoms are not saturated, as GNRs are stripes of graphene. The edge structures are determined by active edge states. The planner patterns are kept, and there are no edge reconstructions for armchair GNRs. The

zigzag edge reconstructs at high temperature, and they are spontaneously metastable. The GNRs exhibit a higher super capacitor performance when they are prepared in an oxidation reduction method as compared to the pristine multi-walled carbon nanotubes (MWCNTs). The electrolyte ionic accessibility is improved through a reduction and oxidation process having functional groups to generate structural defects and pseudo capacities. The effective surface area is increased by longitudinal unzipping. Hence, the electro-active sites of GNRs are increasing, enabling fast-electrochemical reactions.

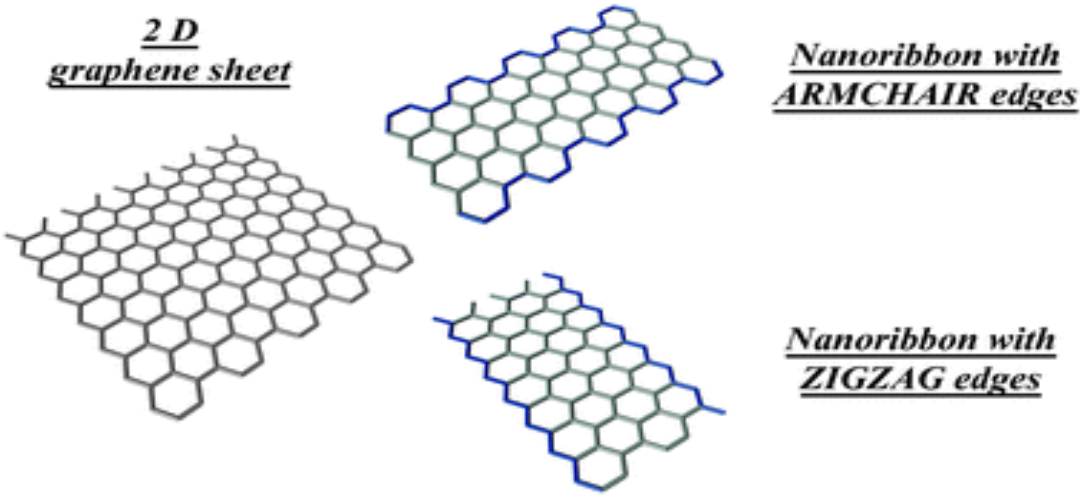

Figure 1.7: Structure of graphene nanoribbons (Adopted with permission, Nanoscale, 3, 2011, 86).

1.2.3.1. Preparation of GNRs

The GNRs are produced from MWCNTs through chemical unzipping. Figure 1.8 shows that CNT, during the oxidation process, is unzipped longitudinally more than any other direction. This is because the red bonds can be easily unzipped to continue the reaction even if an internal tendency to expand is found in the CNTs. On the other hand, there is a reaction of potassium permanganate with C=C in any position.

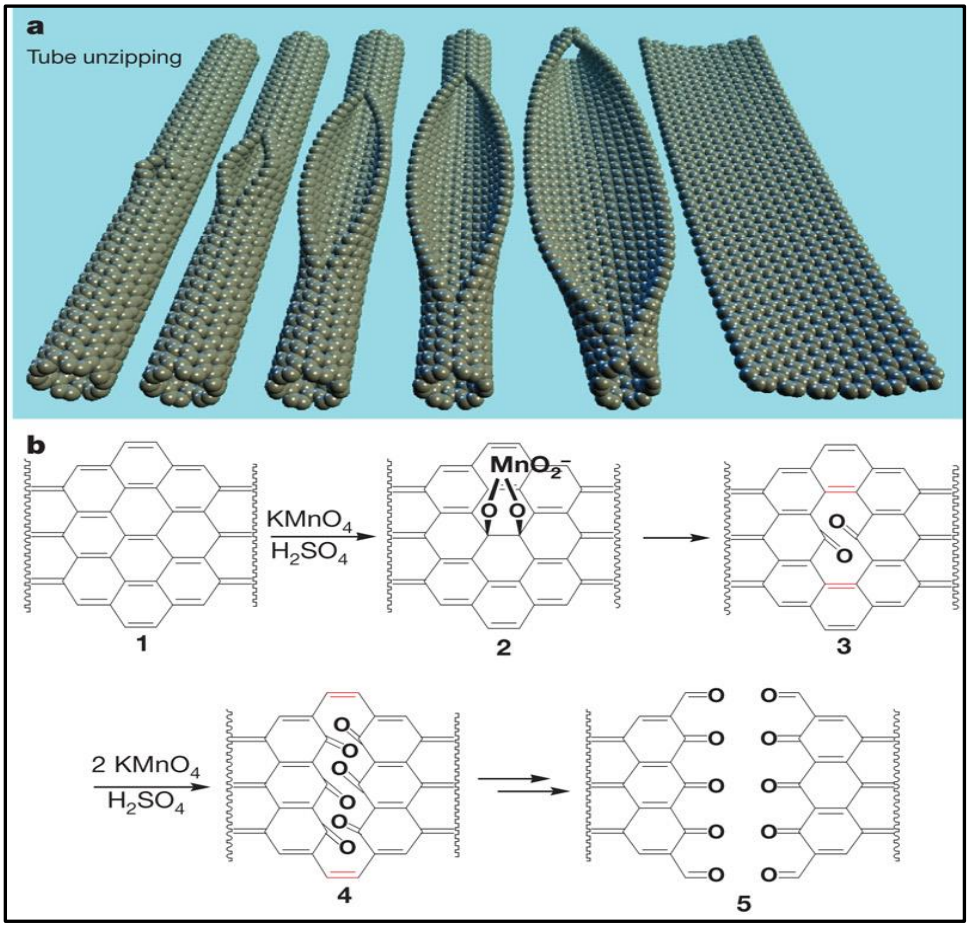

Figure 1.8: Representation of the gradual unzipping of one wall of a carbon nanotube to form a nanoribbon (Adopted with permission, Nature 458, 2009, 872).

1.2.4. Nanocomposites

Nanocomposites are solid materials having multiple phases, and one of these phases contains single, double or three dimensional molecular structures of sizes of few nanometers. Looking at these materials in a wider perspective, they can include porous materials, colloids, gels or polymers.

The main purpose of developing composite material electrodes is to combine the various characteristics into the single electrode so that its capacitance and stability can be improved. For example, insulating polymers can be made conductive by making their

composites with carbon nanotubes. The following is a list of properties that improve the functioning of polymer nanocomposites:

- Electrical conductivity
- Optical clarity as compared to the traditional polymers
- Chemical resistance
- Thermal stability.

1.2.5. Synthesis of nanocomposites

Nanocomposites of polymers with carbon-based materials can be mainly synthesized by three methods. These methods include in-situ polymerization, melt blending and solution casting. The process of in-situ polymerization involves thorough mixing of nano reinforcement and monomer at the initial stages, which leads to monomer polymerization. Similarly, melt blending uses an internal mixer or extruder. The extensive mixing of nano reinforcement and polymer in the extruder results in the formation of nanocomposites. In this method, thermal energy is used for developing polymer mobility. The solvent casting involves the mixing of a solvent, a polymer and a nano reinforcement combined together by a process called ultra-sonication. The result of this process is the development of a nanocomposite in a form of thin film, after the evaporation of solvent.

1.3 Objectives of this work

CPs have been identified as highly conductive, fast charge/discharge, low cost, and environmentally friendly electrode materials for supercapacitors. However, they suffer from lack of stability, and therefore possess limited cycle life. Stability of the CP electrode is limited by degradation through oxidation (they will undergo mechanical/chemical changes, e.g., swelling, shrinkage, cracks or breaking) during long term charge-discharge

processes and as a consequence, gradually their properties are aggravated. In this situation, introducing conducting polymers into the carbon materials could be a good strategy to achieve an optimal capacitive property.

The objectives of this research are:

- Synthesis of graphene nanoribbons by unzipping carbon nanotubes
- Synthesis of graphene nanoribbons/polypyrrole composites with excellent electrochemical properties
- Study the effect of composition on the structural and electrochemical properties of nanocomposites
- Utilizing these materials for energy storage applications.

CHAPTER II

EXPERIMENTAL DETAILS

2.1. Synthesis of unzipped graphene oxide

Graphene nanoribbons were synthesized by unzipping CNTs. For this, 1 g of MWCNTs with outer diameters of 110-170 nm was reacted with 10 g of potassium permanganate (1:10) mass ratio MWCNT to potassium permanganate in a vigorously-stirred mixture of concentrated sulfuric acid [280 ml] and concentrated phosphoric acid [32 ml] in 9:1 acid ratio. The reaction was carried out at 65^{o} C for 4 h. After that, the reaction mixture was cooled to room temperature and poured over ice water (800 ml) containing hydrogen peroxide (40 ml, 30 %). The resulting mixture was congealed overnight then filtered (through 0.2 mm mesh PTFE from Millipore), and washed in succession with hydrochloric acid (30 %), ethanol (100 %), and diethyl ether (anhydrous). The final black material was dried at low heat (65 ^{o}C) in a vacuum oven overnight.

2.2. Synthesis of polypyrrole

Polypyrrole was synthesized using a chemical polymerization process. First, pyrrole (0.8 mol, 1.67 ml) was dissolved in 30 ml of a water and ethanol mixture (1:1, v/v) and then sonicated for 30 min, followed by addition of ferric chloride solution (0.8 mol ferric chloride in 20 ml of water, 2.6 g) dropwise under vigorous stirring for 24 h. Finally,

the obtained material was washed several times with a mixture of water and ethanol until the solution became colorless, and dried in a vacuum at 75 ^{o}C for 24 h.

2.3. Synthesis of nanocomposites

For the synthesis of nanocomposites, first, synthesized graphene nanoribbons were dispersed in 50 ml DI water under ultrasonication for 30 min. in another beaker, pyrrole (0.08 mol) was dissolved in 30 ml of water and ethanol mixture (1:1). The resultant solution was then added to the dispersion of GO solution under ultrasonication for another 30 min. After that, ferric chloride solution (0.04 mol ferric chloride in 20 ml of water) was added dropwise to the above mixture under vigorous stirring for 24 h. The PPy/GO composites obtained were washed several times with a mixture of water and ethanol until the solution became colorless, and dried in a vacuum at 75 ^{o}C for 24 h. The weight ratios of pyrrole to graphene nanoribbons were varied as 99.5 : 0.5, 98.5 : 1.5, 97 : 3, and the resulting nanocomposites were denoted as 0.5PPyGO, 1.5PPyGO, and 3PPyGO. For comparison, the neat PPy was also polymerized by a similar method without addition of GO.

2.4. Characterizations

The synthesized materials were characterized using variety of techniques such as X-ray diffraction (XRD), Scanning Electron Microscopy (SEM), Raman spectroscopy, Fourier Transform Infrared Spectroscopy (FTIR), Thermogravimetric analysis (TGA), BET surface area and pore size distribution measurement techniques, and electrochemical measurements. Details about the characterization techniques are given below:

2.4.1. Scanning electron microscopy (SEM)

Electron microscopes are usually used for observation and classification of the materials on a nanometer (nm) to micrometer (μm) scale. Applications of SEM are important

for the improvement of scientific theories and in progression of materials science and technology. The surface morphology of the GO, PPy, and PPyGO nanocomposites was characterized by using electron microscopy (SEM; QUANTA-200) at University of Memphis. The geometry of a typical scanning electron microscope is shown in Figure 2.1.

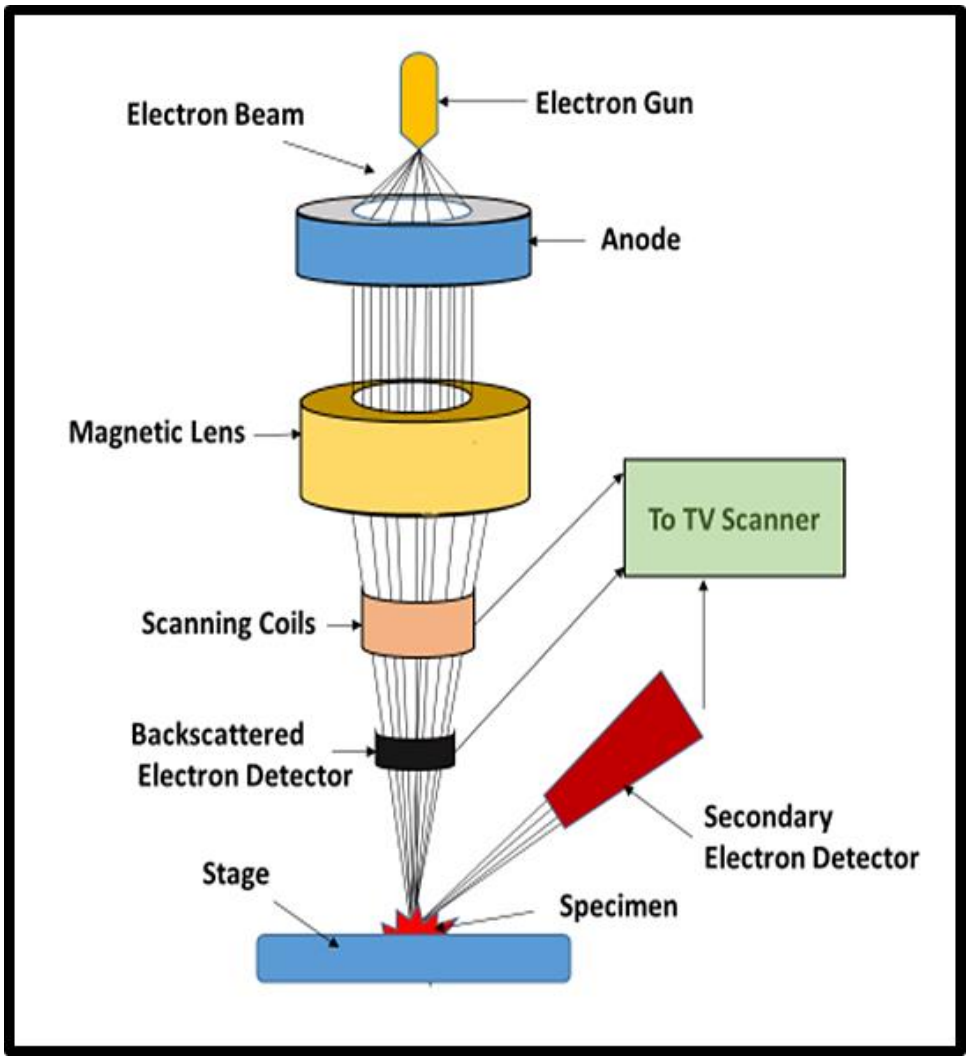

Figure 2.1: Geometry of SEM.

2.4.2. X-ray diffraction (XRD)

Structural examination of synthesized materials was performed through a Shimadzu X-ray diffractometer. The diffractometer was set on the 2θ-θ scan setting with radiation of CuKα1 (λ=1.5406 Å). Slits of 0.3 mm were applied for the source and detector sides. A voltage of 40 kV and a current of 30 mA were applied for X-ray generation. Then, diffraction patterns in the form of X-ray counts were collected utilizing a detector. The sample was rotated through 2θ = 8° - 80° for this collection. Then, geometry was investigated through positioning the X-ray detector in such a way that the angle between the atomic planes and the detector was 2θ. Figure 2.2. illustrates the process.

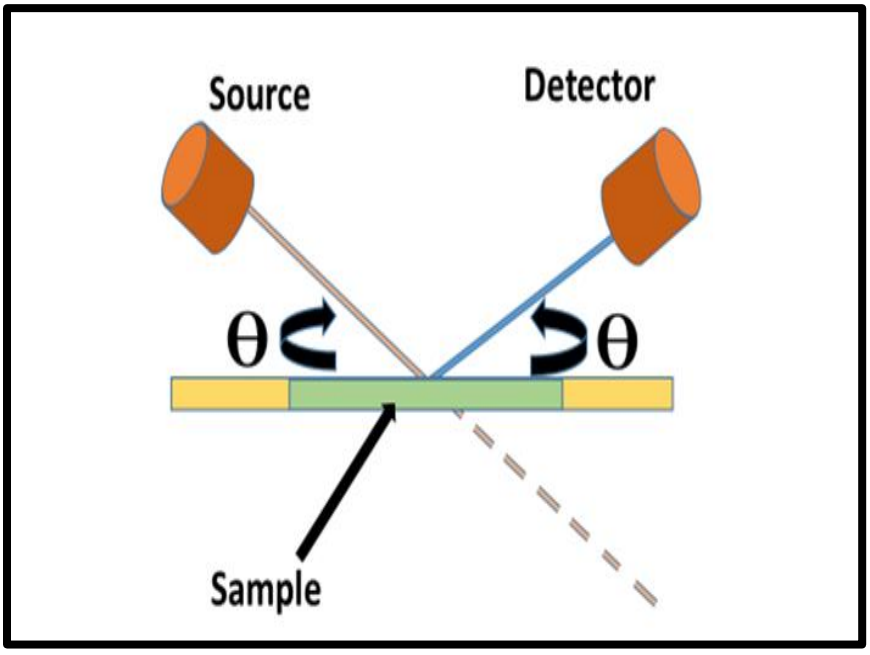

Figure 2.2: Schematic diagram of an X-ray diffractometer.

2.4.3. Raman spectroscopy

The structural characterization of GO, PPy, and their nanocomposites was further performed using Raman spectroscopy. Raman studies were carried out using an argon ion

laser with a wavelength of 514.5 nm as the excitation source (Model Innova 70, Coherent) at University of Memphis.

2.4.4. Fourier transform infrared spectroscopy (FTIR)

FTIR is an analytical method for identifying organic, polymeric, and inorganic materials. In such analysis, scanning of test samples and observation of their chemical properties is done through infrared light. FTIR spectroscopy was performed using a Perkin Elmer Spectrum 2 Spectrometer. In this technique, absorption of infrared radiation by a sample versus wavelength is measured. Molecular components and structures of samples are identified through infrared absorption bands. When infrared radiation is applied to a sample material, molecules of that material are excited into a higher vibrational state through absorption of IR radiation. The wavelength of a particular molecule's absorbed light is a function of the energy difference of molecules which are in the rest or excited vibrational states. These absorbed wavelengths by the sample represent the characteristic of the sample's molecular structure. FTIR spectrometer works by using an interferometer for modulating the wavelength from a source of infrared radiation. Through a detector, intensity of reflected or transmitted light is measured as its wavelength's function. Interferogram is a signal obtained from the detector. It is analyzed by a computer by utilizing Fourier transforms to achieve a single-beam infrared spectrum. Presentation of spectra of FTIR is done through plots of intensity versus wavenumber. The reciprocal of the wavelength is labeled as wavenumber, while intensity is presented through plotting percentage of light transmittance or absorbance at each wavenumber. Figure 2.3 describes the process.

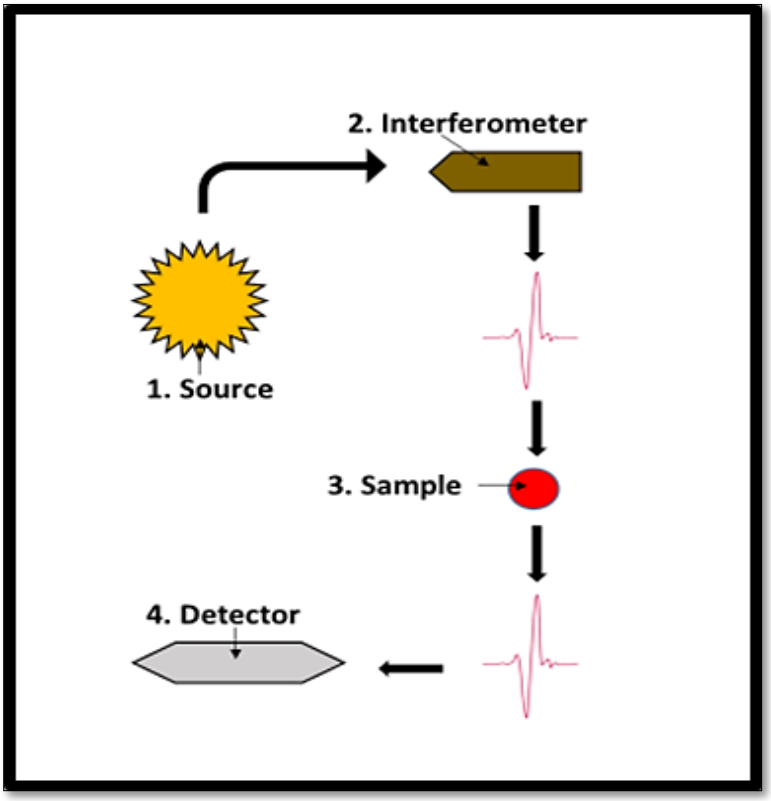

Figure 2.3: Geometry of FTIR.

2.4.5. Surface area and pore size distribution measurement technique

Materials which are utilized for electrodes preparation, such as CPs and nanocomposites, were in the form of dry powder. In order to analyze the surface area of the samples, the technique of physical adsorption of gas on powder surface can be applied. The surface areas of GO, PPy, and PPyGO nanocomposites were determined by the Brunauer-Emmett-Teller (BET) adsorption method (Micrometrics, USA, ASAP 2020 Models). The simple diagram of [BET] is shown in Figure 2.4.

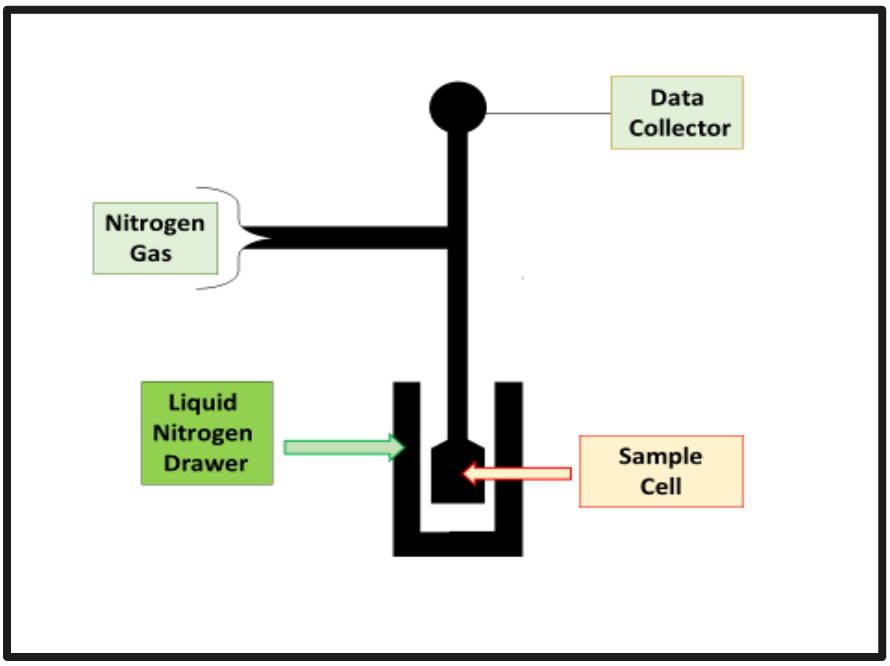

Figure 2.4: Diagram of [BET].

2.4.6. Thermogravimetric analysis (TGA)

The thermal stability of the synthesized materials was determined using a TGA-Q50 thermogravimetric analyzer (TA instruments). In this analysis, the respective sample was placed in a small pan, heated in a controlled manner while connected to a microbalance, and then held isothermally for a specific period of time. The sample is usually kept in an atmosphere of an inert gas like nitrogen. The change in the weight of the sample as a function of temperature is recorded. Figure 2.5 shows the diagram of the process.

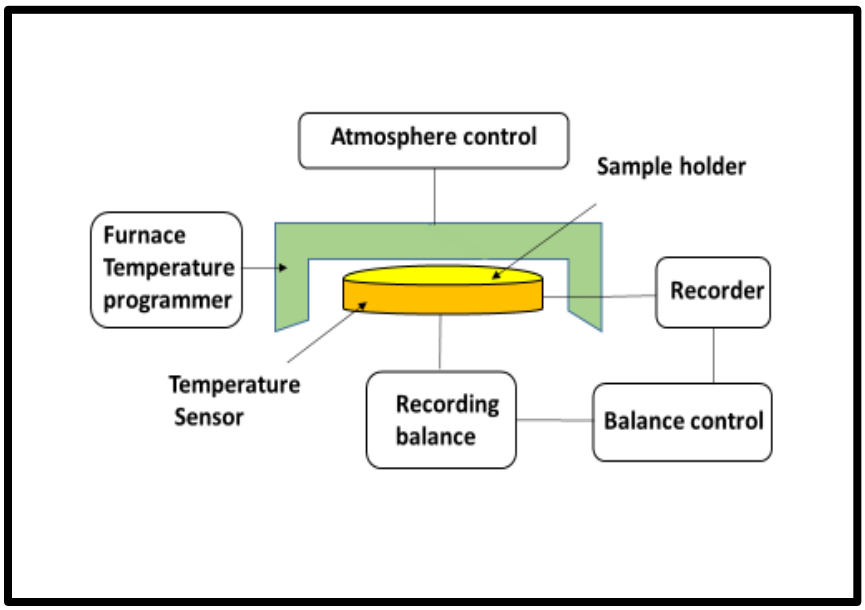

Figure 2.5: Diagram of TGA Instrument.

2.4.7. Electrochemical measurements

A typical three-electrode cell system was utilized for performing electrochemical measurements. In the three-electrode cell system, a reference electrode (a saturated calomel electrode), a counter electrode (a platinum wire) and a working electrode (synthesized nanocomposites on nickel foam) was used. For preparation of a working electrode, first, nickel foam was cleaned using 3M HCl solution, followed by a cleaning using water and acetone. A paste consisting of the synthesized sample (80 wt.%), acetylene black (10 wt.%) and polyvinylidenedifluoride (PVDF, 10 wt.%) was prepared using N-methyl pyrrolidinone (NMP) as a solvent. This paste was then applied on pre-cleaned and weighted nickel foam. The paste was then dried under vacuum at 60 °C for 10 hours. In the process of electrochemical testing a 3M KOH solution was utilized as an electrolyte. The electrochemical testing was performed using an electrochemical workstation (Versastat 4-500) from Princeton Applied Research, USA. In order to examine the electrochemical

attributes of these nanocomposites, cyclic voltammetry (CV) and galvanostatic charge-discharge measurements were performed. Figure 2.6 shows a schematic of a three cell electrochemical measurement system.

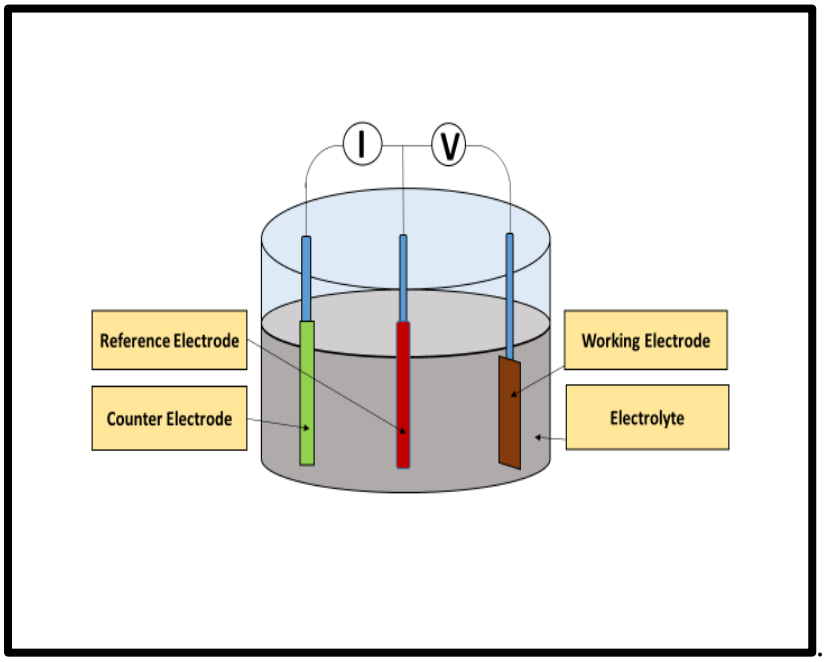

Figure 2.6: Schematic of three cell electrochemical measurement system.

CHAPTER III

RESULTS AND DISCUSSION

3.1. Scanning electron microscopic analysis

The microstructure of polypyrrole and its nanocomposites were analyzed using scanning electron microscopy. The micrographs obtained are shown in Figures 3.1-3.5.

3.1.1. Graphene and polypyrrole

The micrograph of pure GO reveals that the layers of GO are densely stacked as coralline-like flakes of irregular dimensions. On the other hand, the SEM micrograph for a pure PPY as shown in Figure 3.2 shows that a segregation of PPy nanoparticles took place to form a cauliflower-like structure as obtained in the previous studies as well [24].

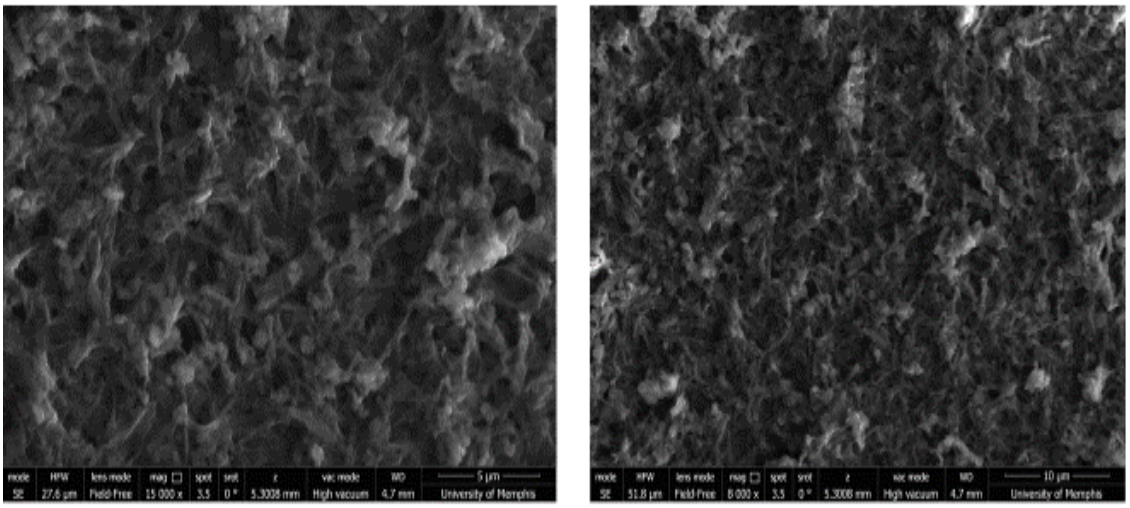

Figure 3.1: SEM images of GO at various magnifications.

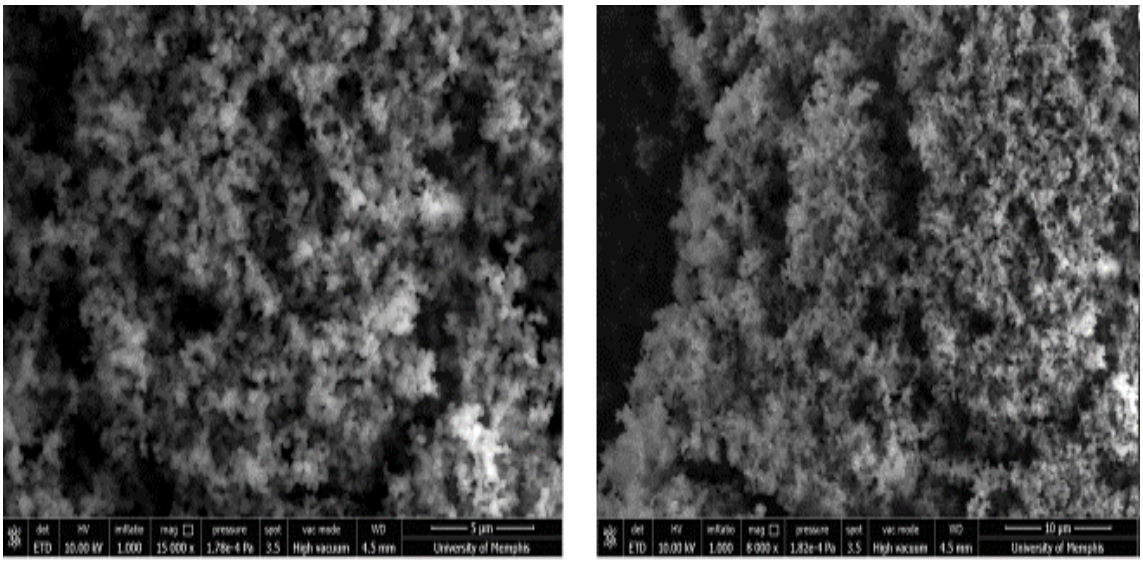

Figure 3.2: SEM images of PPy at various magnifications.

3.1.2. PPYGO Composites

The micrographs in Figures 3.3-3.6 are of the three composites of polypyrrole and graphene nanoribbons (0.5, 1.5, and 3 PPYGO respectively). It is evident from these images that the addition of PPy led to a uniform growth of its nanoparticles on the GO

flakes. Such phenomena could be a result of intense interaction (such as physical forces, hydrogen bonding, and pi-stacking etc.) between GO and PPy [25]. Some aggregates of PPy nanoparticles could also be seen in the 3PPyGO composite. With an increasing concentration of PPy, the roughness of stacked GO increased and a large variety of pores were established [26]. Such surface features can significantly improve the charge transfer characteristics and capacitance of the PPyGO electrode [27].

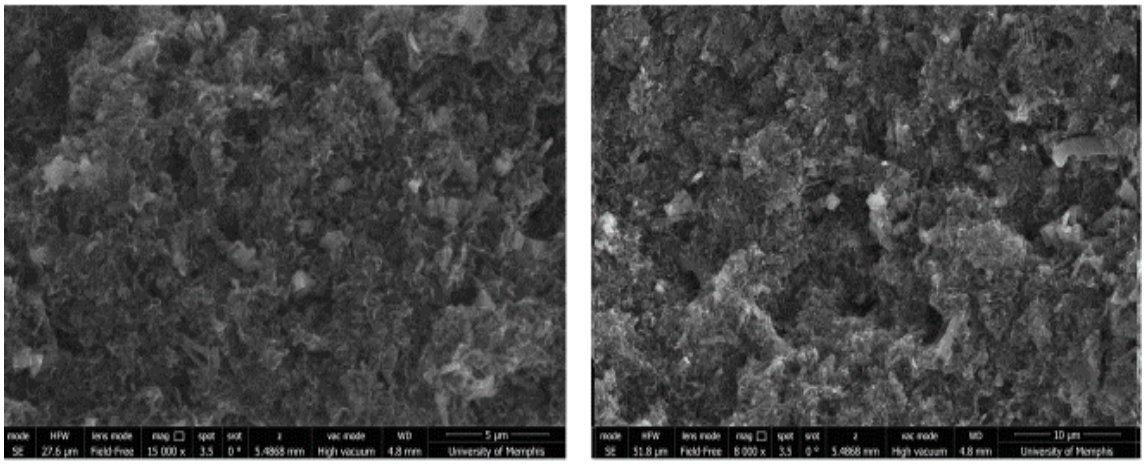

Figure 3.3: SEM images of 0.5PPyGO at various magnifications.

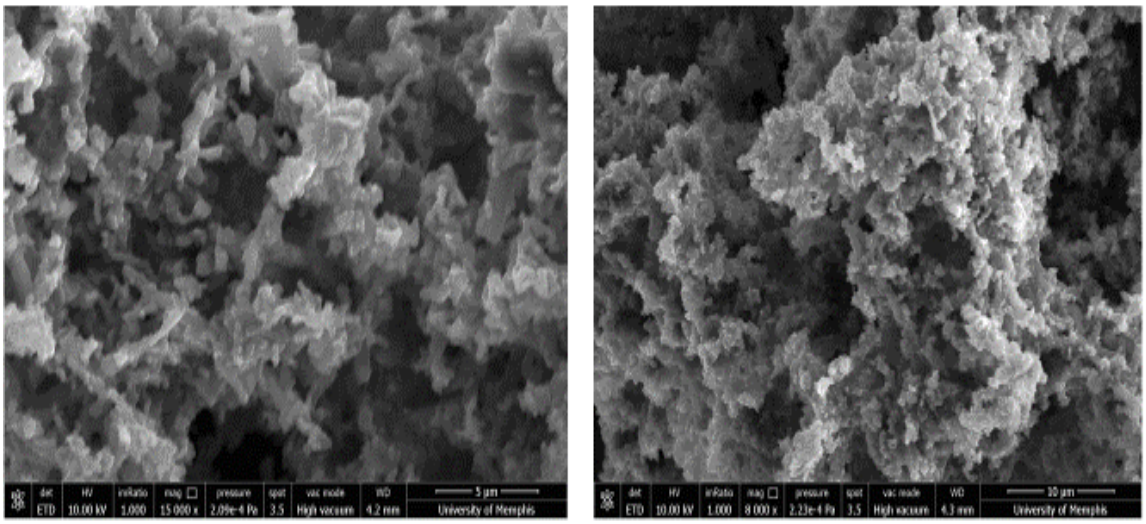

Figure 3.4: SEM images of 1.5PPyGO at various magnifications.

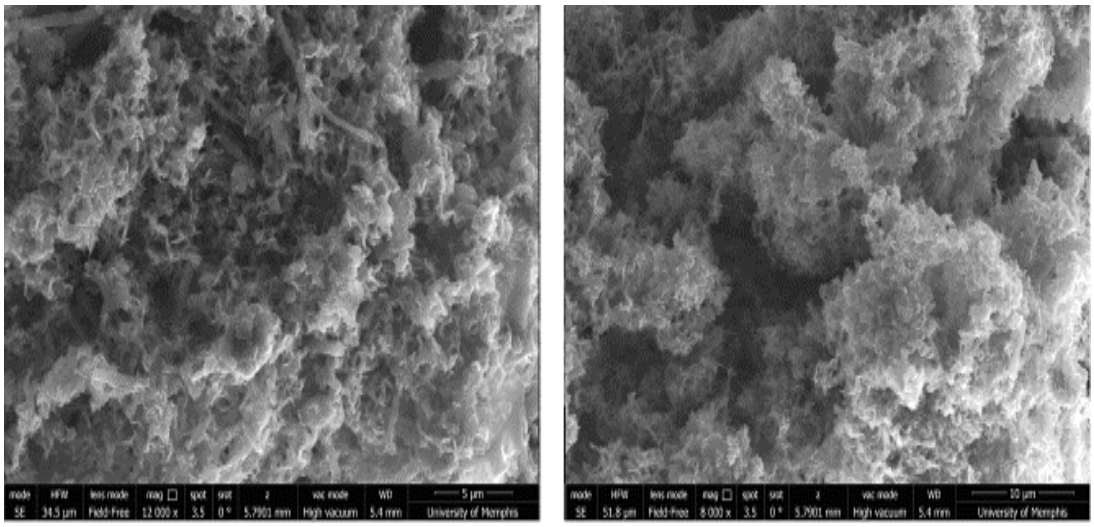

Figure 3.5: SEM images of 3PPyGO at various magnifications.

3.2. X-ray diffraction analysis

3.2.1. CNT, graphene and polypyrrole

The unzipping and exfoliation of MWCNT to form unzipped graphene nanoribbons was investigated by using XRD studies. Figures 3.6.-3.8 show the XRD patterns of CNTs, GO and PPy, respectively. In the case of CNTs, the diffraction peaks in the vicinity of 25°, 45°, and 55° can be related to the (002), (100), and (004) planes of hexagonal graphite structure, respectively [28]. The formation of GO was investigated by using XRD studies. Like the earlier studies, a strong reflection was obtained around $2\theta=10^{o}$ corresponding to an interlayer spacing of 8.47 A^{o}. In the case of GO, the shifting of (002) peak to low intensity can be related to the attachment of residual functional groups having oxygen. These functional groups were bonded to the GO sheets and they led to an increase in the interlayer spacing of graphitic structure [25]

The diffraction patterns for pure PPy gave a broader peak in the region of $2\theta= 20^{o}$ to 28^{o} and this indicated the formation of amorphous phase of PPy.

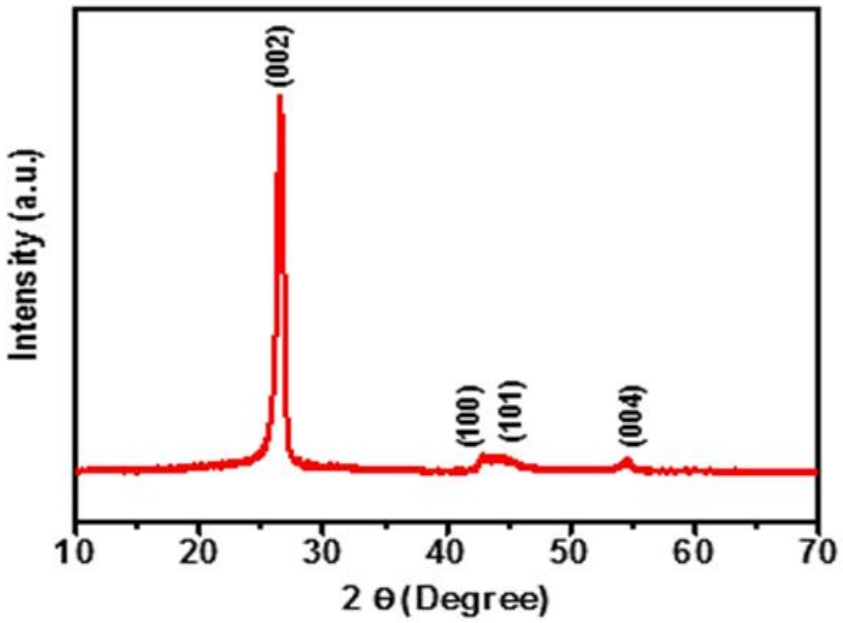

Figure 3.6: XRD of CNT.

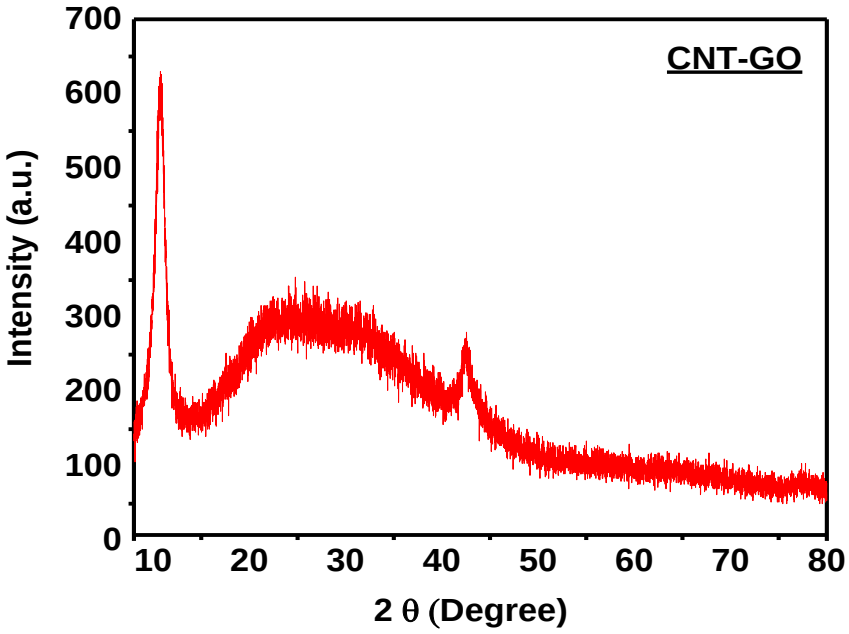

Figure 3.7: XRD of graphene nanoribbons.

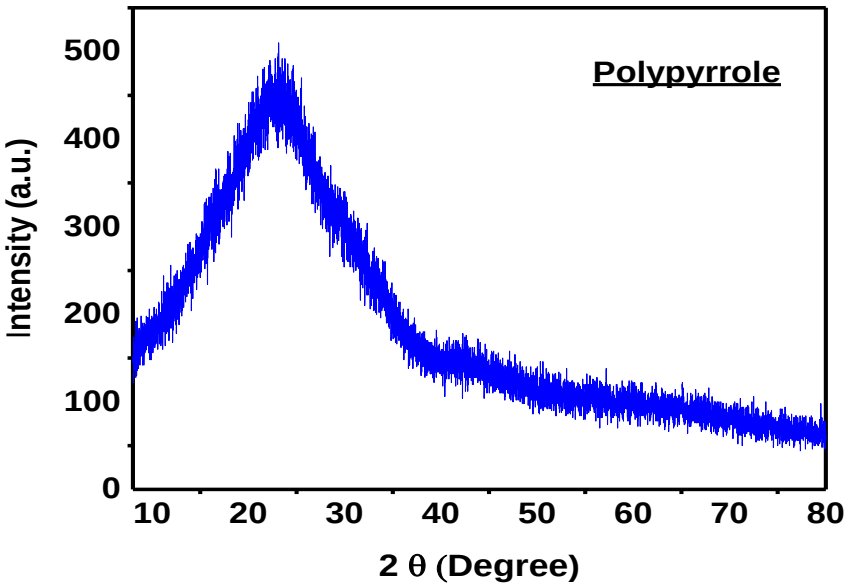

Figure 3.8: XRD of polypyrrole.

3.2.2. PPyGO composite.

The diffraction patterns of the three composites are shown in Figures 3.9-3.11. As before with the PPY, a similar diffraction peak in the region of 2θ= 20^{o} to 28^{o} was obtained. However, no diffraction peak was obtained for GO. This could be due to the complete covering of GO sheets by PPy [25].

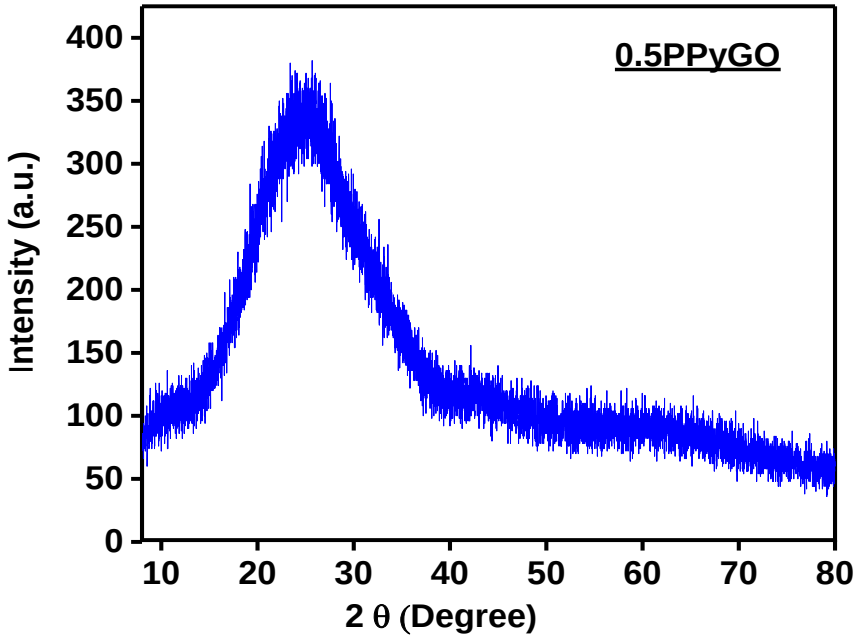

Figure 3.9: XRD of 0.5PPyGO.

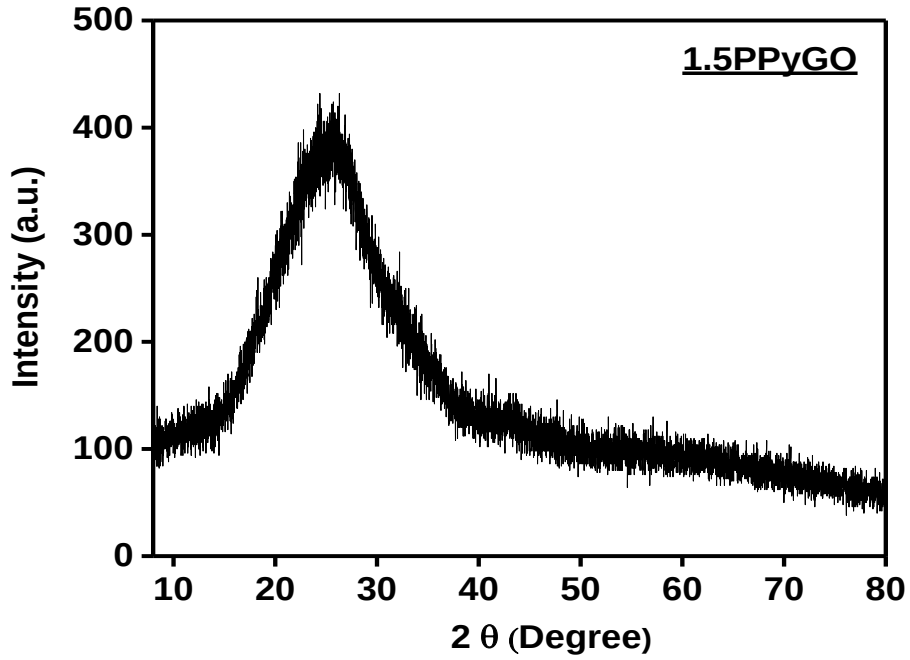

Figure 3.10: XRD of 1.5PPyGO.

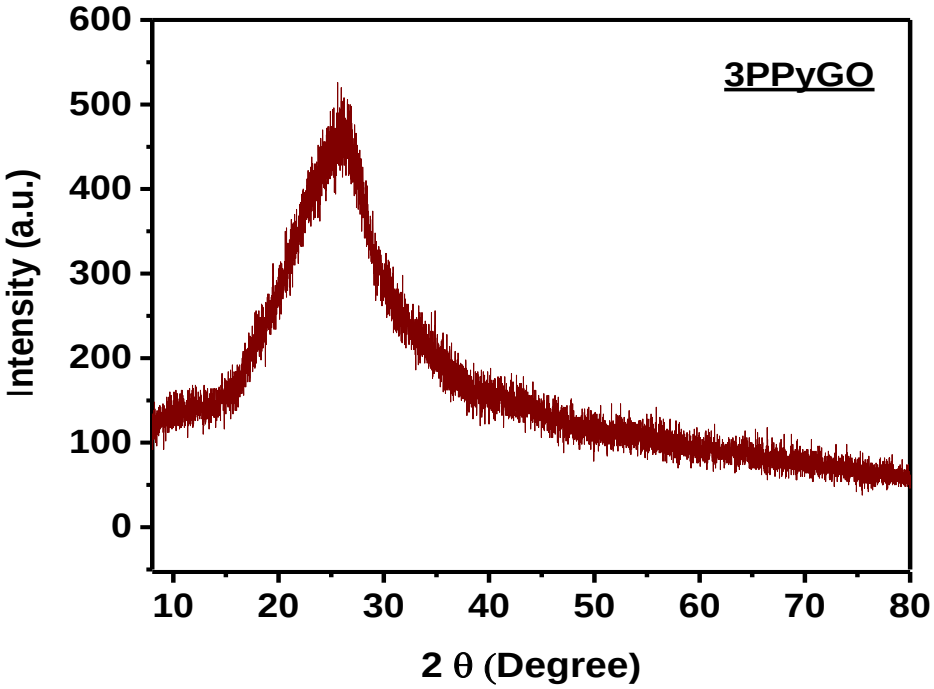

Figure 3.11: XRD of 3PPyGO.

3.3. Raman spectroscopy

3.3.1. Graphene and polypyrrole

The results of Raman spectroscopy of GO and PPy are shown in Figures 3.12-3-13. The Raman spectrum was recorded in a frequency range of 0 to 3500 cm^{-1}. The spectrum of GO shows two high intensity bands (G and D) at around 1586 cm^{-1} and 1345 cm^{-1}. These bands are related to the in-plane optical vibration of graphite lattice and the first-order scattering of zone boundary phonons (E_{2g} mode) [24, 29]. In the case of PPY, intense bands at around 555 cm^{-1} and 1050 cm^{-1} were obtained. These bands indicate the C-H out-of-plane and in-plane the formation of PPY backbone [30].

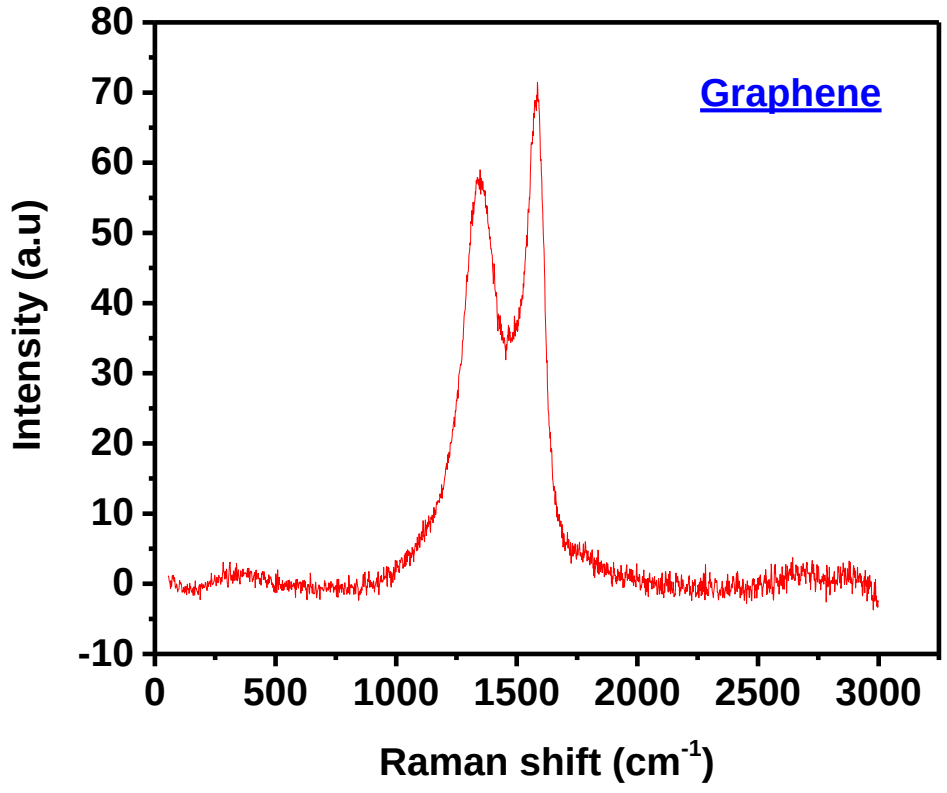

Figure 3.12: Raman spectrum of GO.

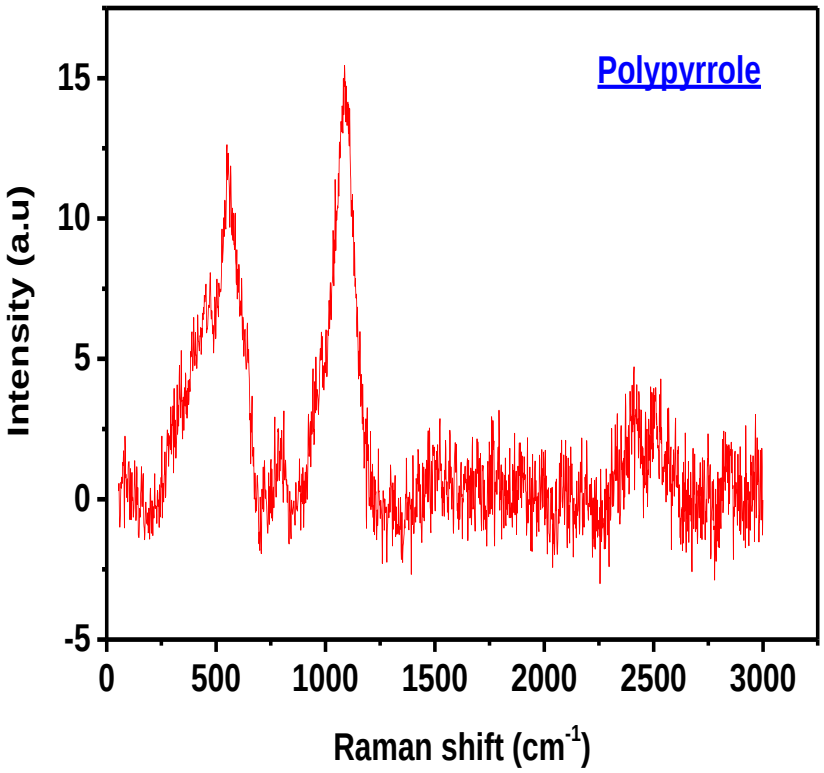

Figure 3.13: Raman spectrum of PPy.

3.3.2. PPyGO composites

The Raman spectra of the three composites are given in Figures 3.14-3.16. The obtained bands in the spectra of three composites had values of around 1560 cm^{-1} and 1340 cm^{-1}. They can be related to the π-π interaction between the rings of PPy and the stretching vibration of its backbone, respectively. For all three samples, the broadness of bands can be attributed to the interaction of PPy with GO sheets [30,31].

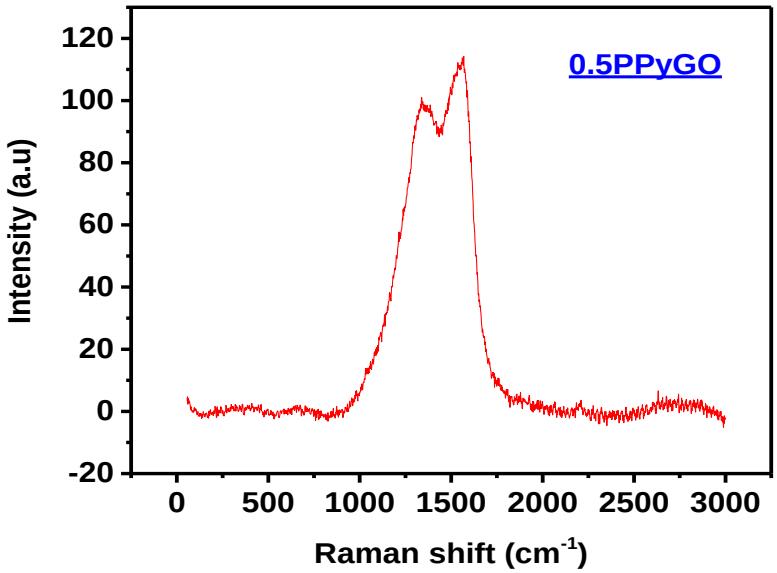

Figure 3.14: Raman spectrum of 0.5PPyGO.

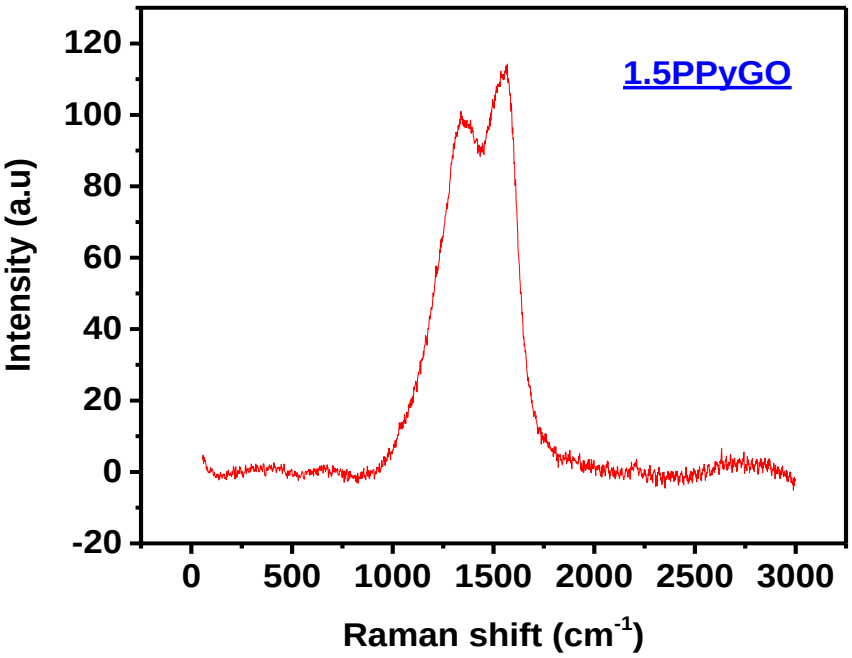

Figure 3.15: Raman spectrum of 1.5PPyGO.

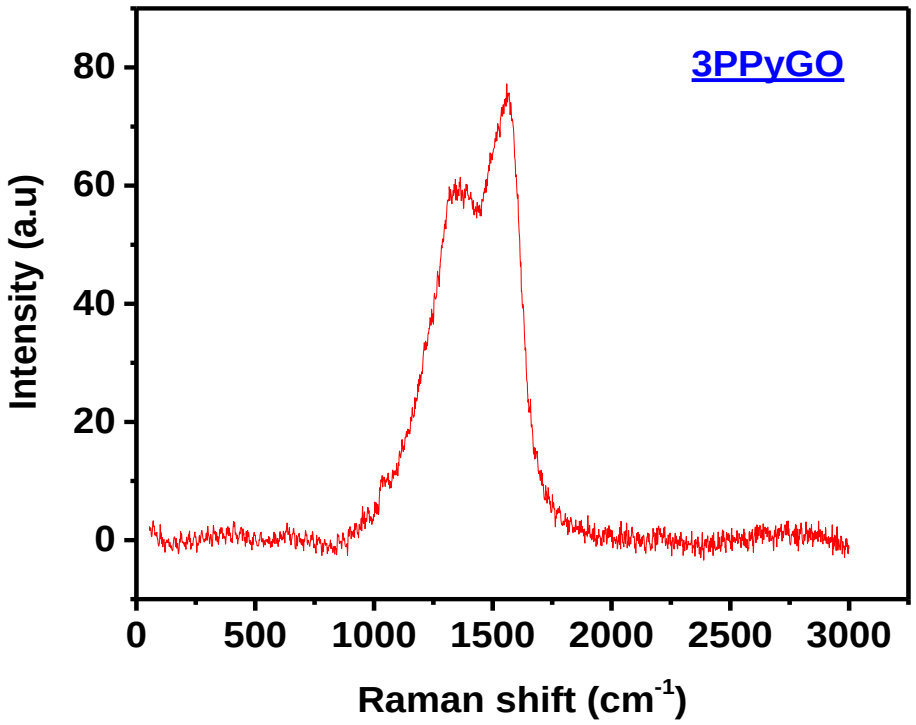

Figure 3.16: Raman spectrum of 3PPyGO.

3.4. Fourier transform infrared spectroscopy (FTIR)

3.4.1. Graphene and polypyrrole

Figures 3.17-3.18 show the FTIR spectra of pure GO and PPy. In the case of GO, the peaks obtained at 1732 cm^{-1} and 1038 cm^{-1} are associated with the stretching vibrations of carboxylic (C=O) and alkoxy (C-O) groups attached around the edges of a GO sheet. In addition, the peak at 1617 cm^{-1} is attributed to the skeletal vibration of unoxidized GO. The broad absorption peak obtained at 3300 cm^{-1} indicates the hydrogen-bonded hydroxyl group [32].

The FTIR spectra of PPy shows a strong peak at 1558 cm^{-1}, which corresponds to a PPy symmetric ring vibration. The two strong peaks at 1217 cm^{-1} and 1051 cm^{-1} could

be attributed to the N-C stretching and the N-C vibration band. The presence of polymerized PPy is affirmed by the strong peaks at 937 cm^{-1}, 771 cm^{-1}, and 710 cm^{-1} [25, 33]. They normally indicate the out-of-plane bend of C-H vibration band [34].

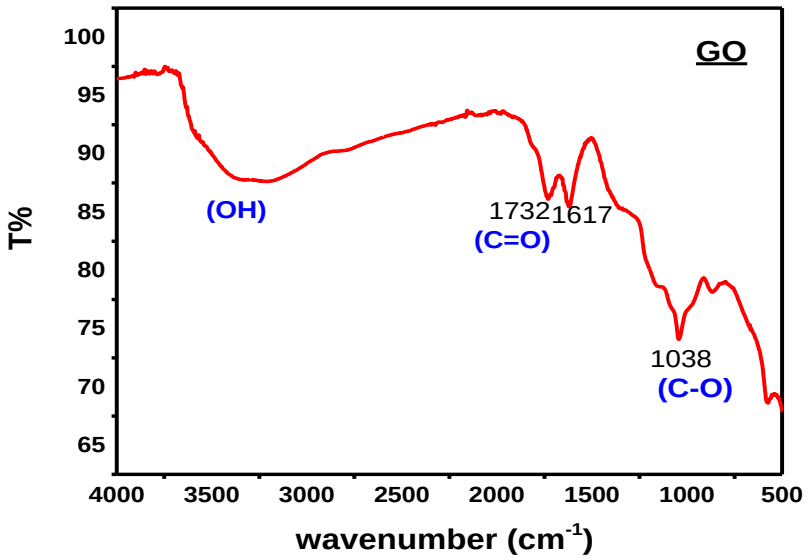

Figure 3.17: FTIR of graphene nanoribbons.

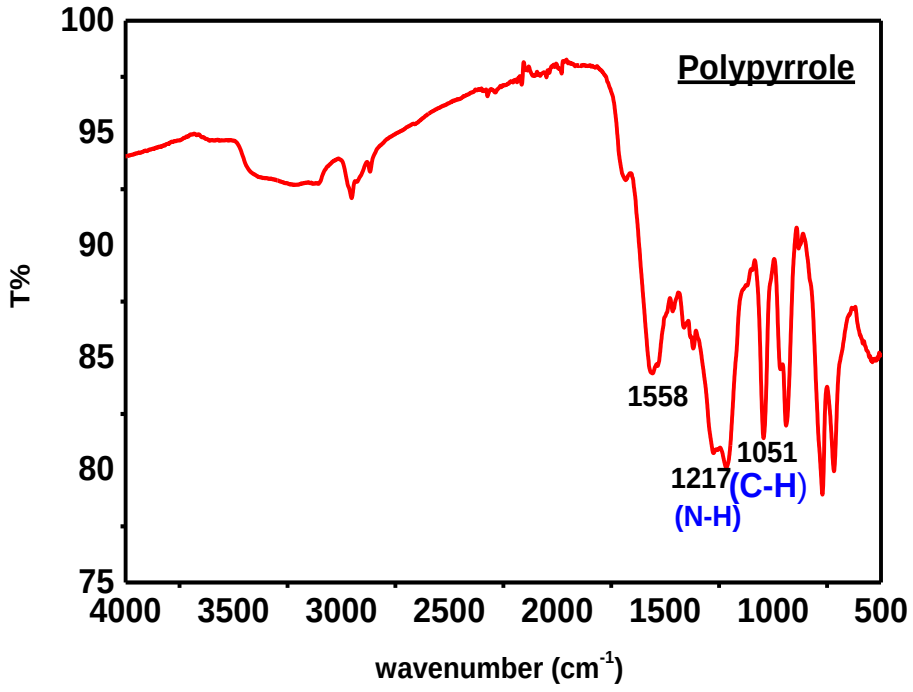

Figure 3.18: FTIR of polypyrrole.

3.4.2. PPyGO composites

The FTIR results of the three composite samples are shown in Figures 3.19-3.21. Overall, a clear similarity exists in the spectra of pure PPy and composites. All of the PPy characteristic peaks are present in the spectrums of all three composites, and they are independent of the PPy concentration. It should be noted that the peak corresponding to PPy symmetric ring vibration (1558 cm^{-1}) has been shifted to a lower wave number (around 1535 cm^{-1}), and this indicates a π-π interaction between the rings of PPy and unoxidized GO [25,32]. The absence of GO characteristic absorption stretch at 1732 cm^{-1} in spectrums of all three composites signifies that hydrogen bonding has been developed between the amine (N-H) groups of PPy and carboxylic (C=O) groups of GO [25].

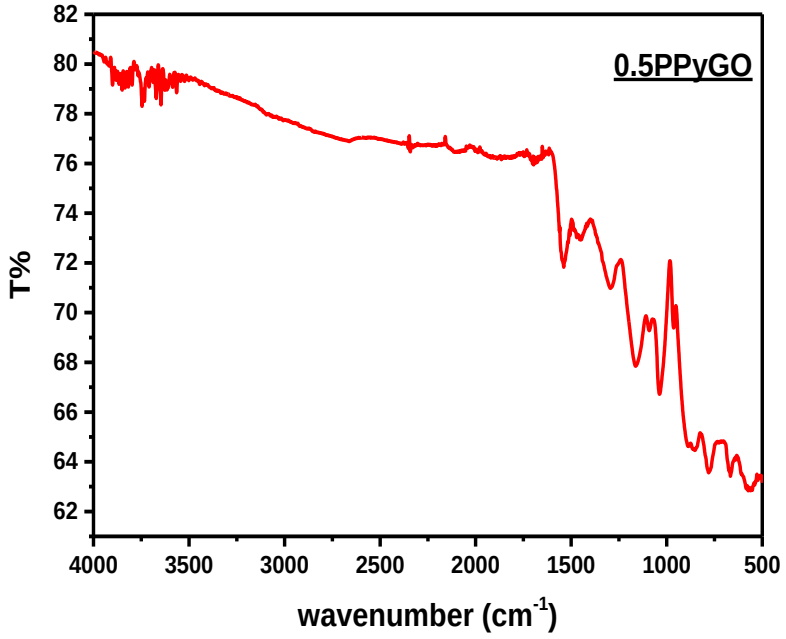

Figure 3.19: FTIR of 0.5PPyGO.

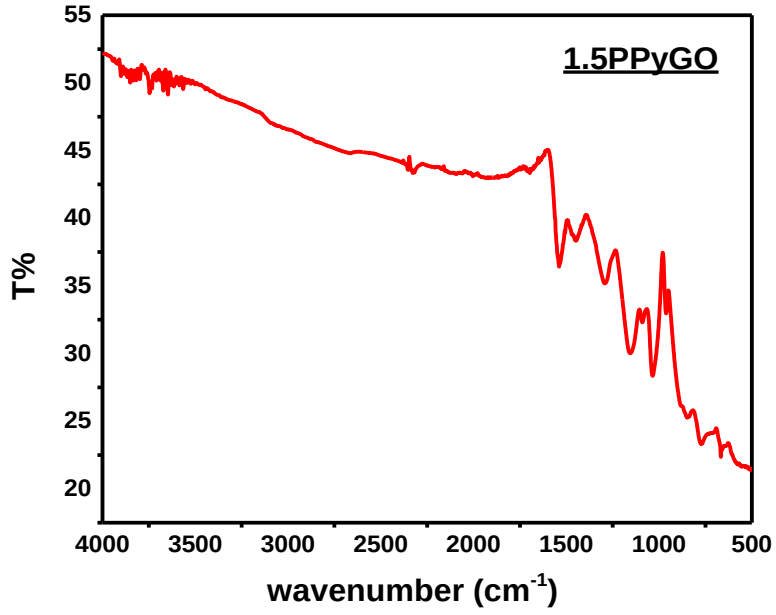

Figure 3.20: FTIR of 1.5PPyGO.

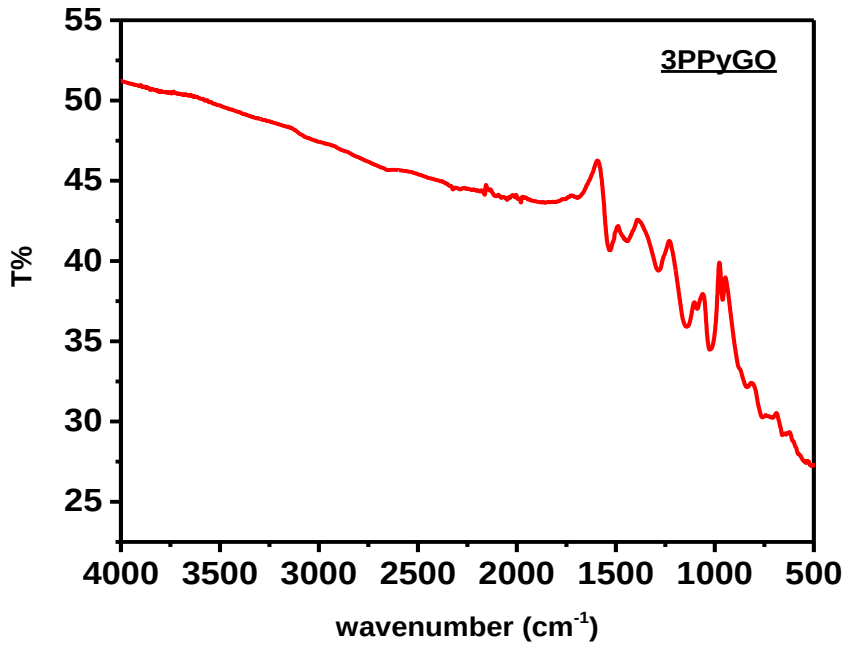

Figure 3.21: FTIR of 3PPyGO.

3.5. Surface area and pore size distribution measurement technique

3.5.1. Graphene oxide

The results of GO obtained from pore size and nitrogen adsorption-desorption studies are shown in Figure 3.22. The Brunaure–Emmett–Teller (BET) surface area was found to be 115 m^2/g. Figure 3.22-a shows the distribution of pore sizes of the prepared samples. This pore size ranged from 20 to 180 nm and this distribution was obtained by using Barret-Joyner-Halenda model. Many of the pore sizes were scattered between 30 nm to 80 nm range.

Figure 3.22-b shows a Type III adsorption isotherm with absence of any hysteresis loop. It is obtained if the value of C in the BET equation is significantly less than unity. This type of isotherm also indicates the formation of a multilayer, and the absence of any flattish portion in the obtained sample signifies the absence of a monolayer.

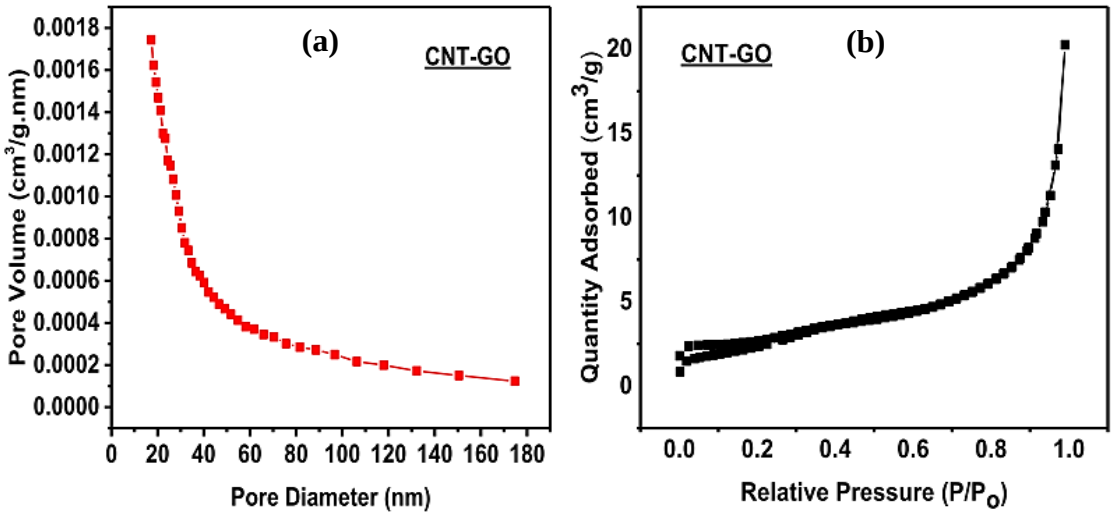

Figure 3.22: (a) Pore size distribution and (b) Nitrogen adsorption/desorption isotherm of the GO.

3.5.2. Polypyrrole

Figure 3.23-a displays the results of PPy obtained from pore-size distribution and BET studies. As with the GO, the pore diameters (Figure 3.23-b) ranged from 20 nm to 180 nm. The major scattering of pore sizes was found to be in the 20-70 nm range. The specific surface of the prepared sample, which was 5.7 m^2/g , was obtained through the BET method. In this case, the adsorption isotherm showed Type II characteristics, and the intermediate region of the curve indicated the formation of a monolayer. Here, slight hysteresis between the adsorption and desorption curves was also present. This indicated the filling and emptying of mesopores having diameters around 20 nm.

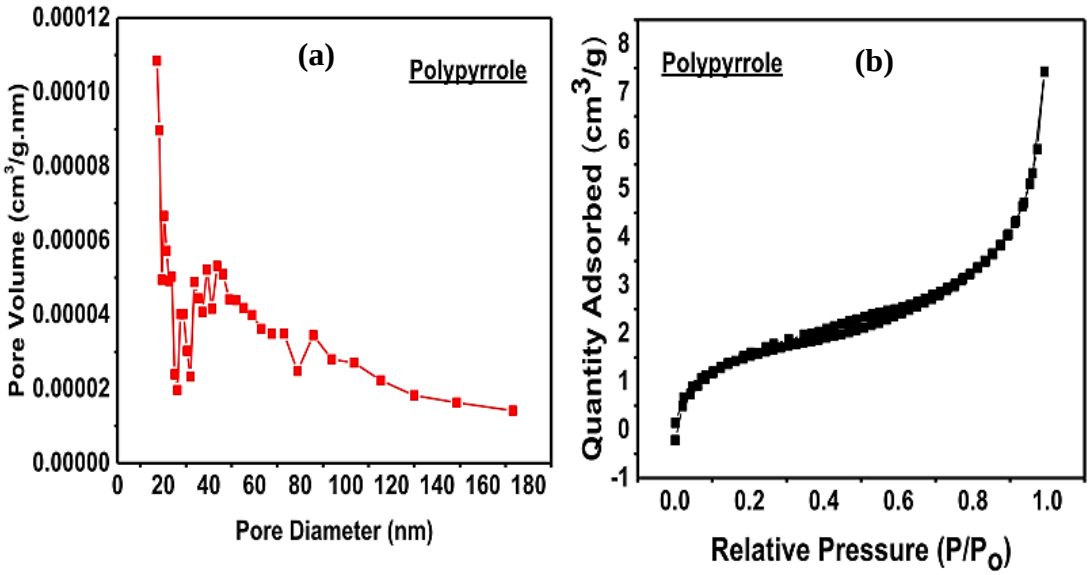

Figure 3.23: (a) Pore size distribution and (b) Nitrogen adsorption/desorption isotherm of PPy.

3.5.3. Polypyrrole and graphene nanocomposites

The results of 0.5, 1.5, and 3PPyGO nanocomposites are shown in Figures 3.24-3.26. The range of pore size distribution (Figures 3.24-a, 3.25-a, and 3.26-a) were the same as before, but generally most of the pores had a smaller diameter in the final composites. The addition of GO led to a significant increase in the specific surface area of PPy, leading to a value of 16.5 m^2/g, 36.3 m^2/g, and 78.2 m^2/g for the final composites. Such an increment in the surface area results in the availability of more active sites on the nanocomposite electrodes. This may also lead to an improvement in the charge storage capacity of the nanocomposites. As before, a Type II absorption (Figures 3.24-b, 3.25-b, and 3.26-b) was obtained and a monolayer formation took place. Here, no hysteresis was obtained between the adsorption and desorption curves.

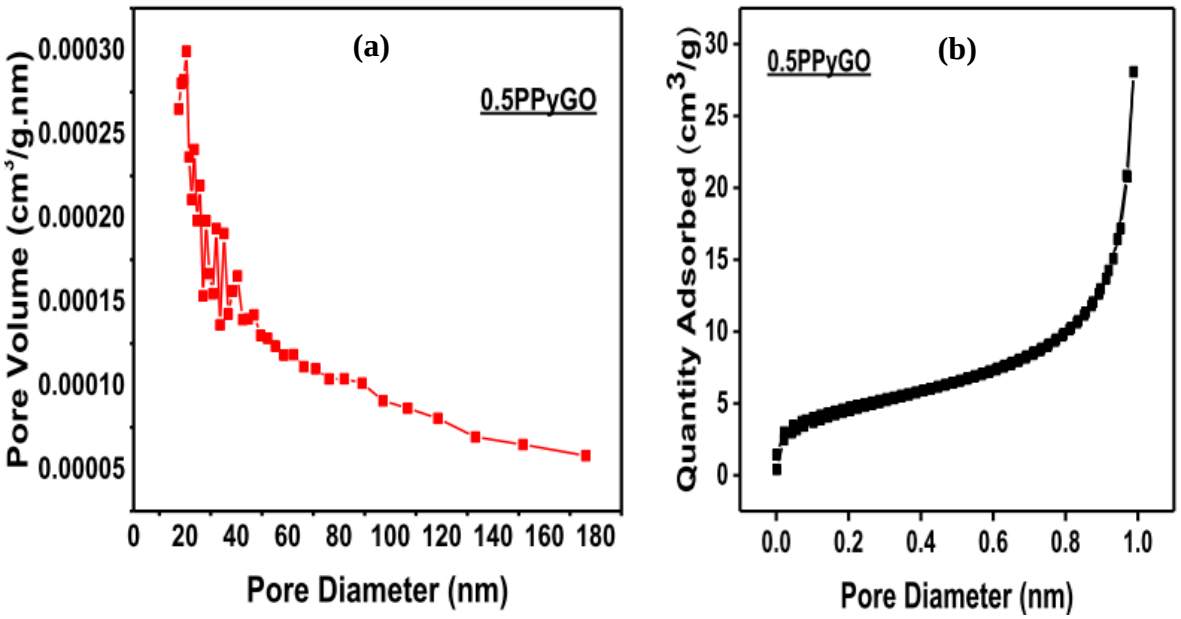

Figure 3.24: (a) Pore size distribution and (b) Nitrogen adsorption/desorption isotherm of the 0.5PPyGO.

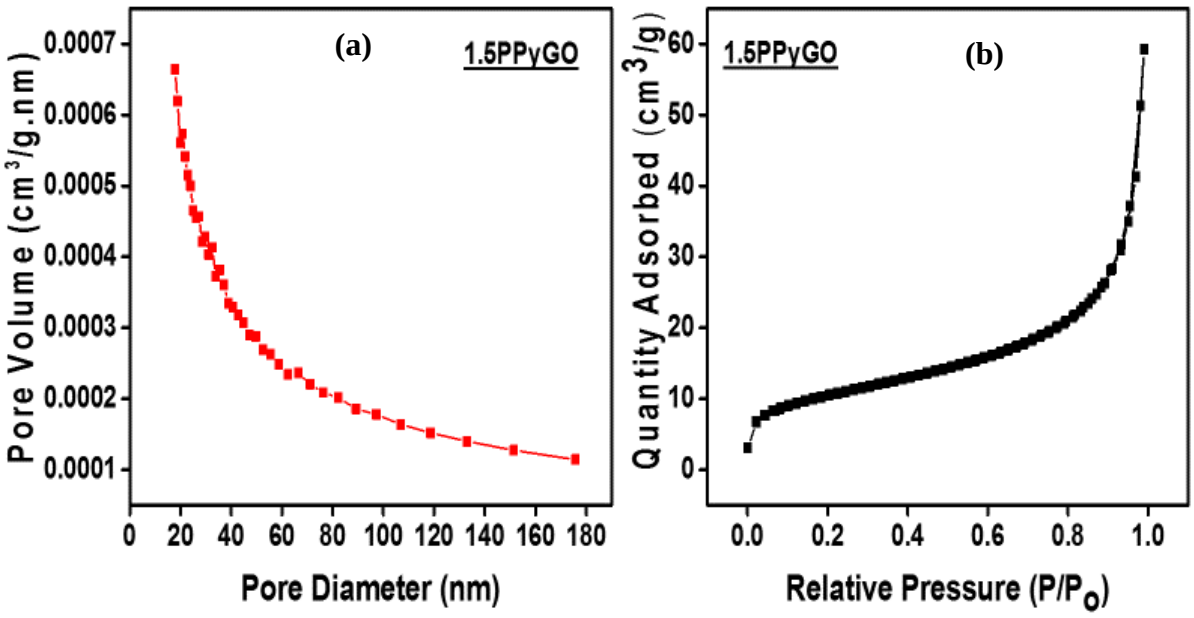

Figure 3.25: (a) Pore size distribution and (b) Nitrogen adsorption/desorption isotherm of the 1.5PPyGO.

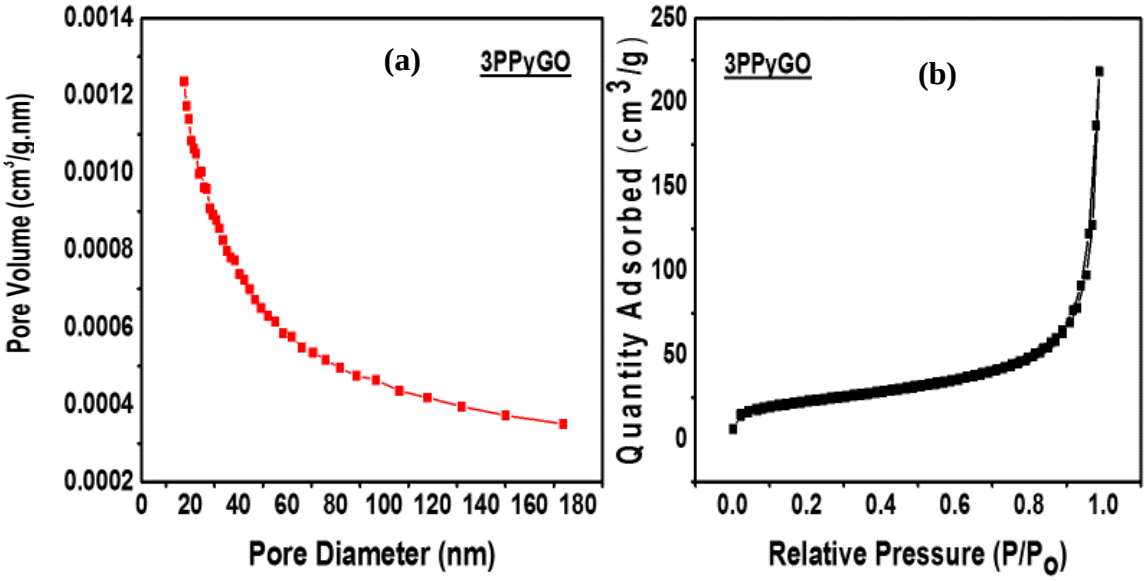

Figure 3.26: (a) Pore size distribution and (b) Nitrogen adsorption/desorption isotherm of the 3PPyGO.

3.6. Thermogravimetric analysis (TGA)

3.6.1. Graphene and polypyrrole

The thermal analysis results of GO and PPy are shown in Figure 3.27. The initial mass loss (around 100 °C) occurred in all samples; this indicates the removal of absorbed water. In the case of GO, major weight loss occurred below 250 °C. At 150 °C, a major weight loss occurred which corresponded to the decomposition of oxygen-containing functional groups on the surface of GO layers [32]. On the other hand, the weight loss around 200°C indicated the decomposition of GO into carbon soot.

The TGA result of PPy (Figure 3.28) shows a uniform weight loss from around 300 °C to onwards because of the pyrolysis of main polymer chains [35].

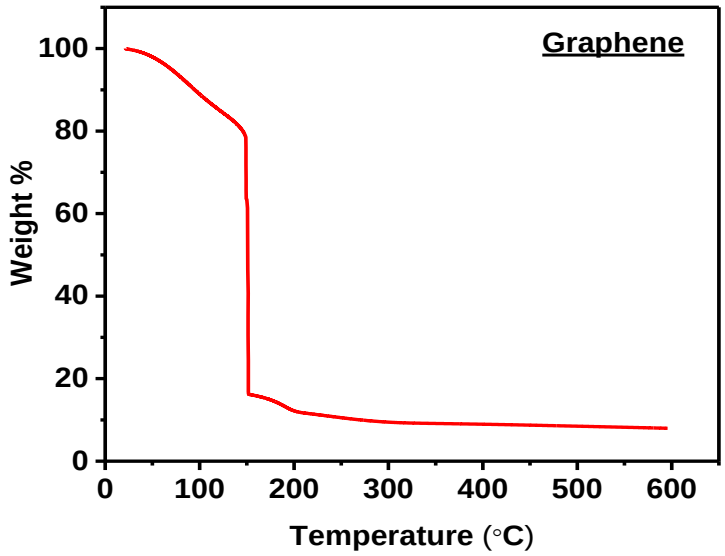

Figure 3.27: TGA of graphene nanoribbons.

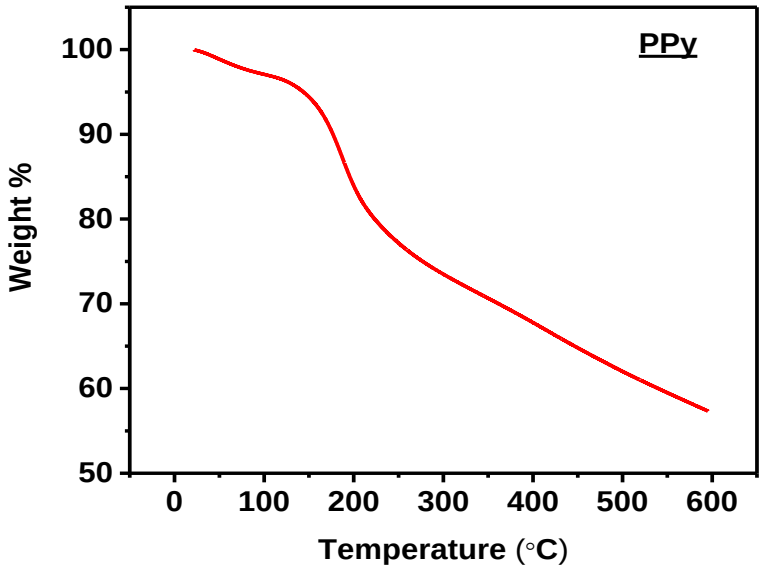

Figure 3.28: TGA of PPy.

3.6.2. PPYGO composites

Figures 3.29-3.31. show the TGA plots of the three composites. As observed in pure material, the initial mass loss occurred due to the removal of absorbed water and, like

the pure PPy, all samples showed a uniform weight loss with no stable intermediates. Such similarities between the TGA profiles suggest a uniform dispersion of PPy nanoparticles on the GO matrix.

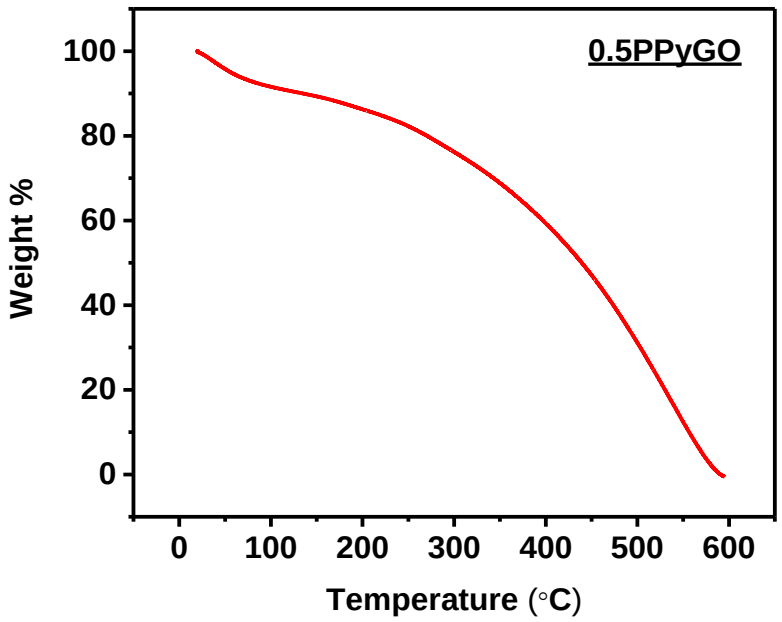

Figure 3.29: TGA of 0.5PPyGO.

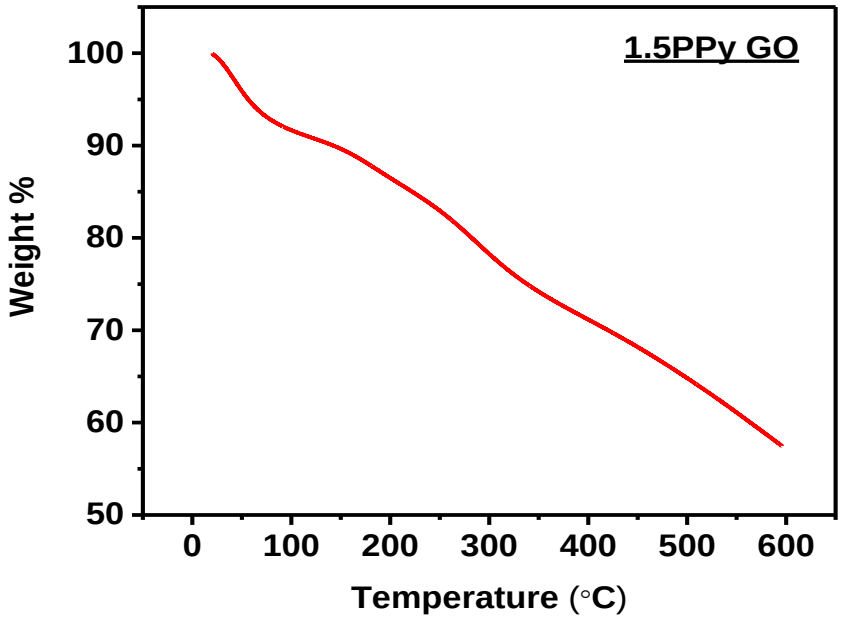

Figure 3.30: TGA of 1.5PPyGO.

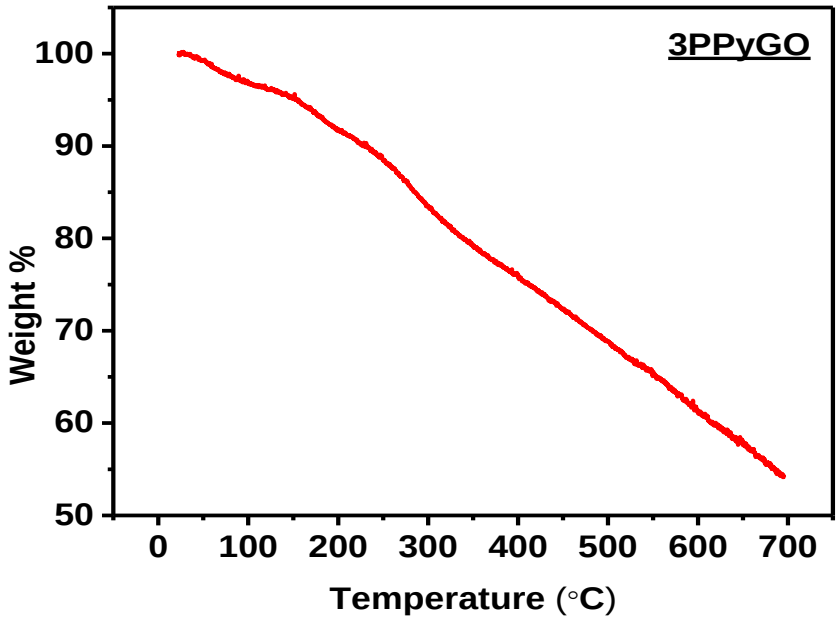

Figure 3.31: TGA of 3PPyGO.

3.6. Electrochemical characterizations

The purpose of this experiment was to study the electrochemical properties of synthesized GO, PPy, and their nanocomposites. Cyclic voltammetry and galvanostatic charge-discharge measurements were performed in 3M KOH electrolytes to investigate their electrochemical properties. Figures 3.32-3.36 show the CV curves of GO, PPy, and their nanocomposites at various scan rates. The existence of redox peaks is evident in the cyclic voltammograms of these samples which indicates that the charge storage process in these systems is dominated by the redox process.

Specific capacitance of these electrode was calculated using the measurements from the cyclic voltammetry data. Following is the expression that was used in calculation of specific capacitance (C_{sp}) of the electrodes.

$$C_{sp} = \frac{Q}{\Delta V \times (\frac{\partial v}{\partial t}) \times m}$$

where, $\partial v/\partial t$ is the scan rate, and Q is the area under CV curve, m is the mass of sample and ΔV is the potential window of CV measurement. Figures 3.37-3.41 indicate the variation in specific capacitances as a function of scan rate for various samples. It was observed that specific capacitance decreases with an increase in scan rate, which could be due to insufficient time for redox reaction at higher scan rates. In this process, electrochemical stability of the electrodes is evident, as the shapes of the CV curves are similar even at high scan rates. It was also observed that, with the increase in scan rate, the peak position was shifted towards a higher potential. It can be inferred that the transfer of charge is the result of diffusion controlled process in these materials.

Table 3.1. on page 55 shows the values of specific capacitance at scan rate for all the samples. The maximum value of specific capacitance was observed to be 2,066 F/g for 3PPyGO. The specific capacitances of 0.5PPyGO and 1.5PPyGO were calculated to be 659 F/g and 1,368 F/g, respectively, which confirms that increasing the amount of GO improves the electrochemical performance of the electrode.

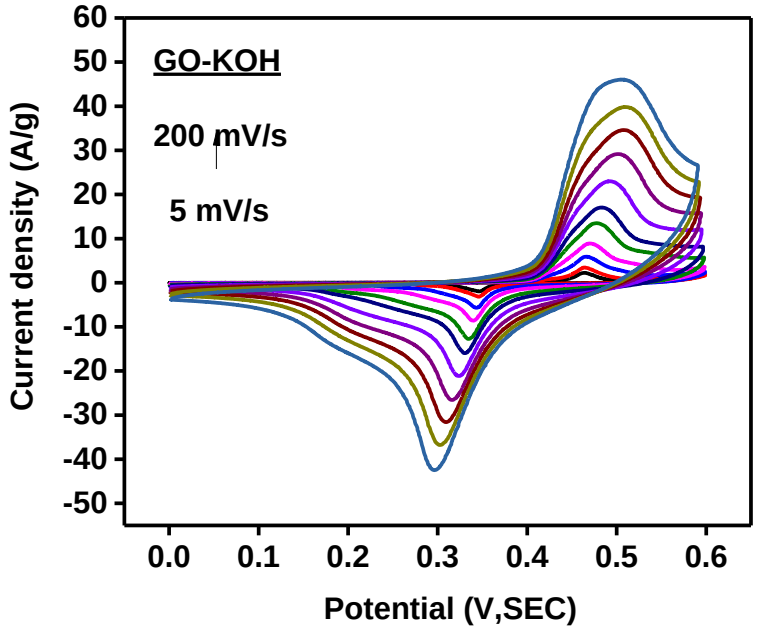

Figure 3.32: Cyclic voltammograms of GO sample at various scan rates in 3M KOH electrolyte.

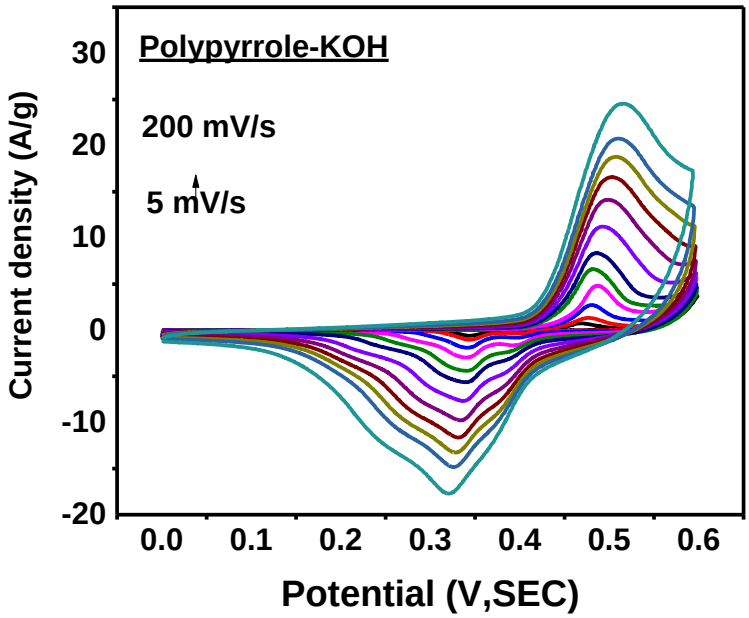

Figure 3.33: Cyclic voltammograms of PPy sample at various scan rates in 3M KOH electrolyte.

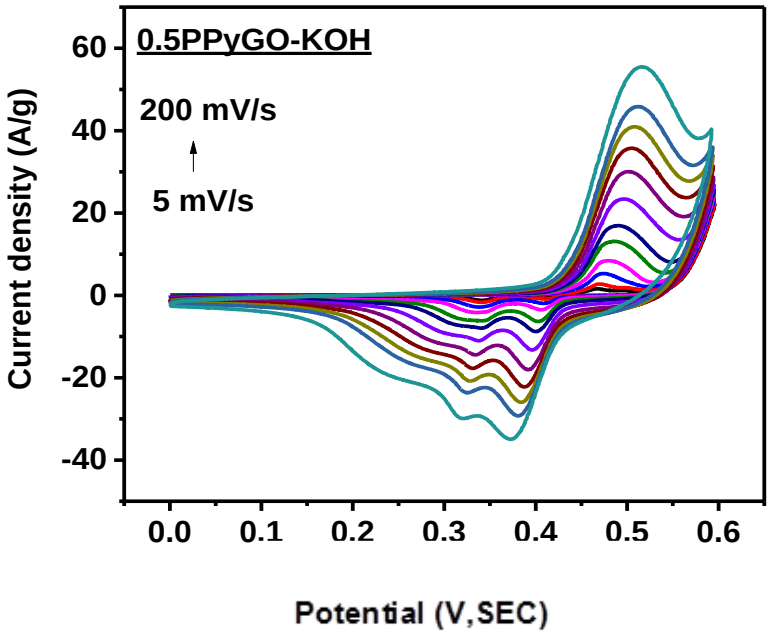

Figure 3.34: Cyclic voltammograms of 0.5PPyGO sample at various scan rates in 3M KOH electrolyte.

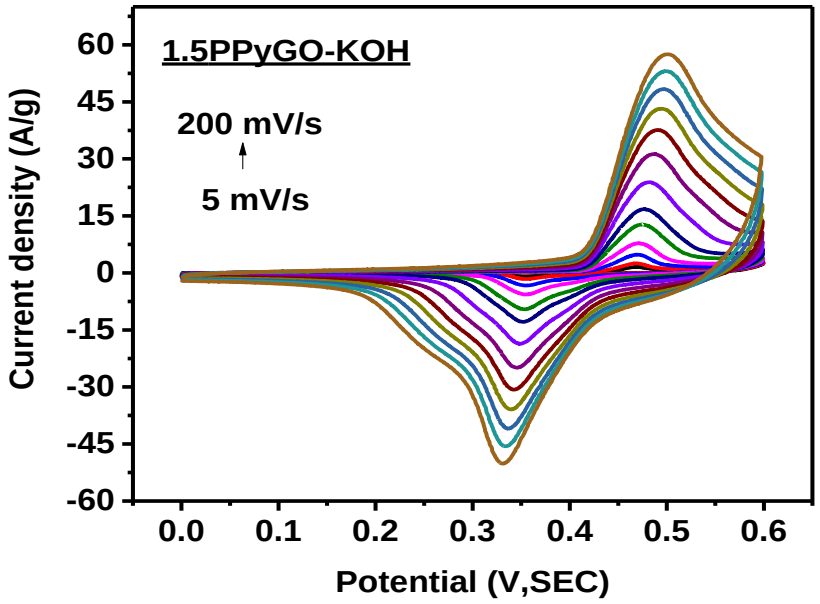

Figure 3.35: Cyclic voltammograms of 1.5PPyGO sample at various scan rates in 3M KOH electrolyte.

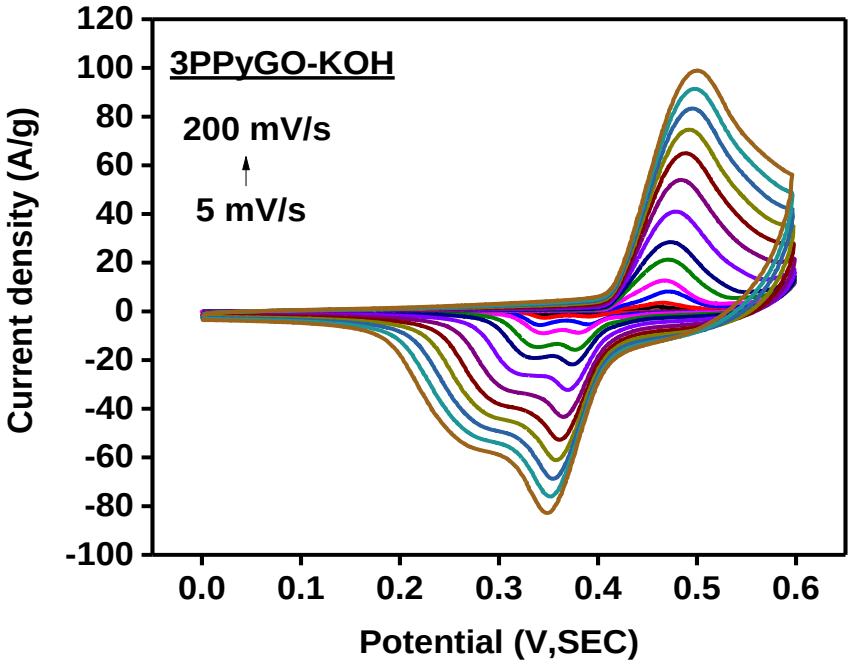

Figure 3.36: Cyclic voltammograms of 3PPyGO sample at various scan rates in 3M KOH electrolyte.

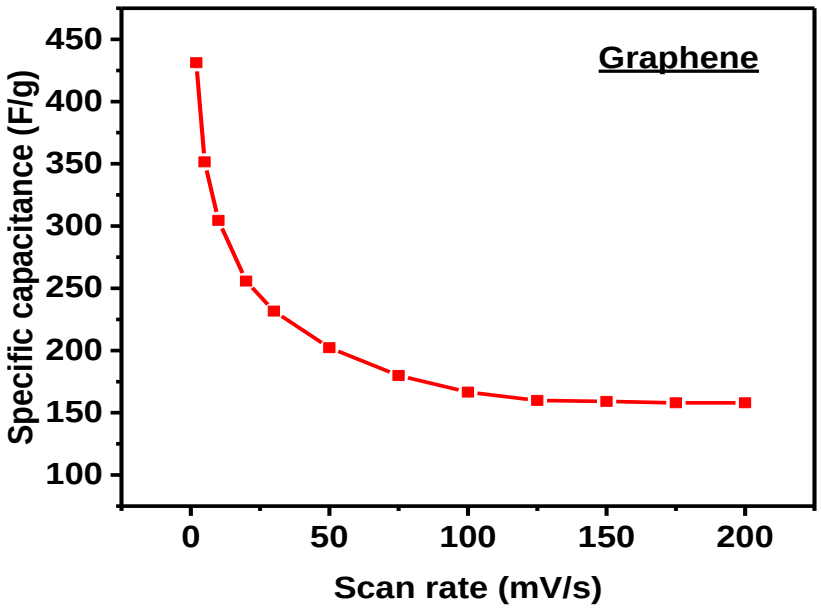

Figure 3.37: Specific capacitance as a function of scan rate for GO sample in 3M KOH electrolyte.

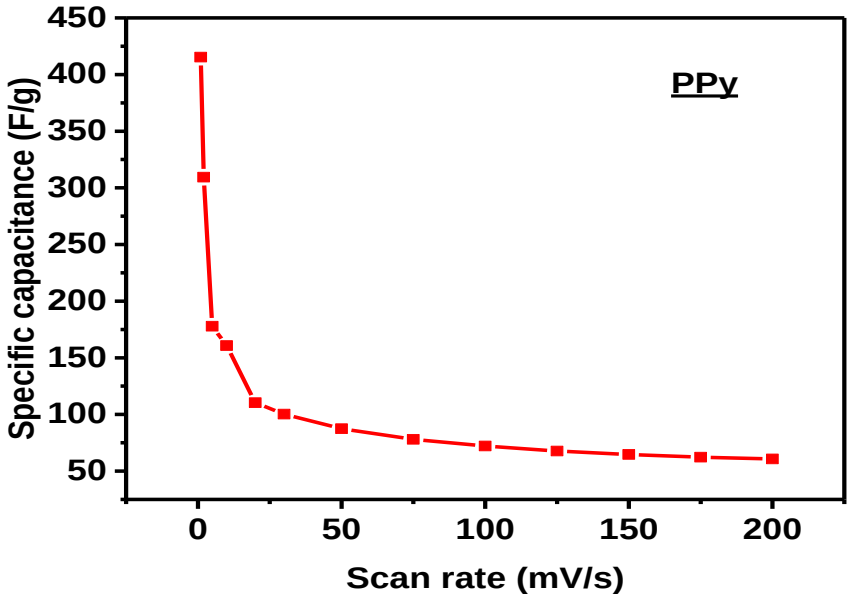

Figure 3.38: Specific capacitance as a function of scan rate for PPy sample in 3M KOH electrolyte.

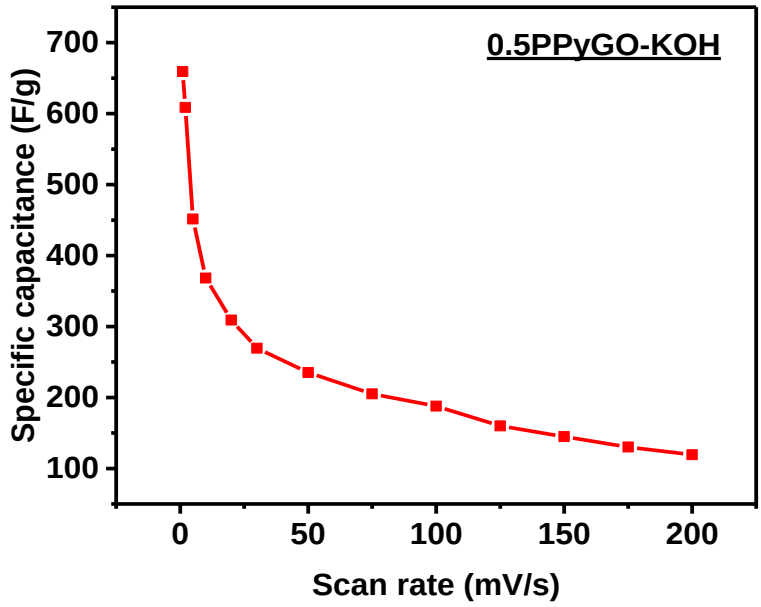

Figure 3.39: Specific capacitance as a function of scan rate for 0.5PPyGO sample in 3M KOH electrolyte.

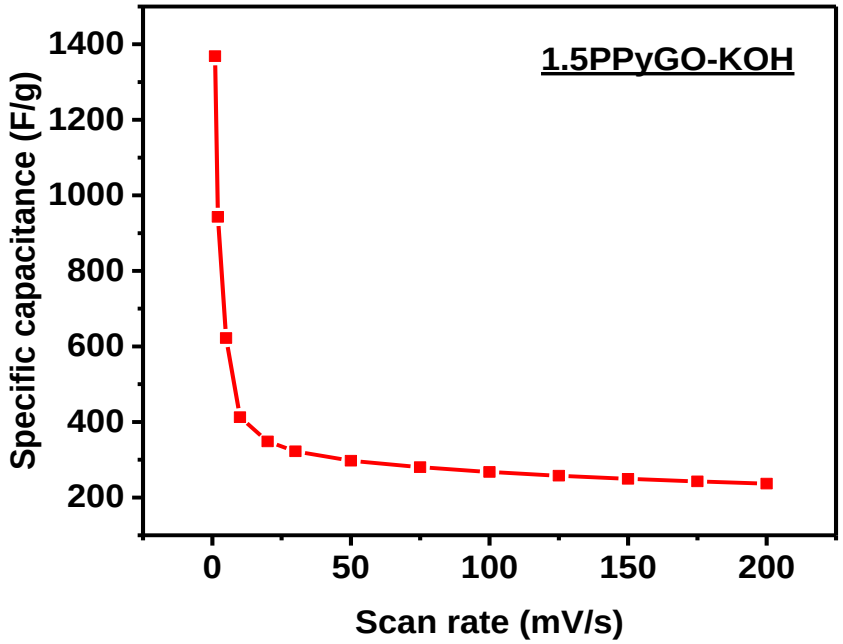

Figure 3.40: Specific capacitance as a function of scan rate for 1.5PPyGO sample in 3M KOH electrolyte.

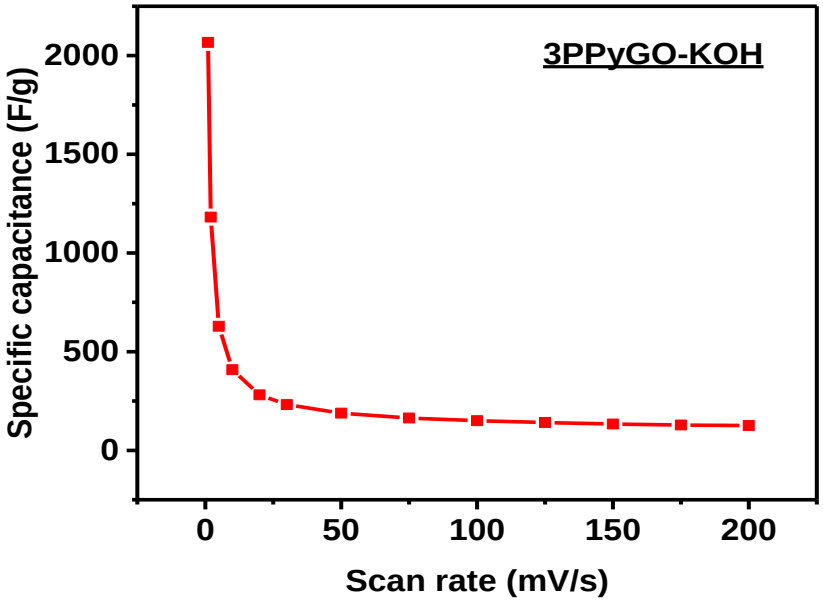

Figure 3.41: Specific capacitance as a function of scan rate for 3PPyGO sample in 3M KOH electrolyte.

Table 3.1: Comparison of GO, PPy and PPyGO nanocomposites in specific capacitance as a function of scan rate electrochemical performance.

Sample	specific capacitance Vs. scan rate
Polypyrrole	**415 F/g**
Graphene	**443 F/g**
0.5PPyGO	**659 F/g**
1.5PPyGO	**1368 F/g**
3PPyGO	**2066 F/g**

3.6.1. Galvanostatic charge-discharge measurements

In order to evaluate the potential application of the nanocomposites for the purpose of energy storage devices, the galvanostatic charge-discharge measurements were performed. These measurements were performed in 3M KOH electrolyte. The potential window selected was 0-0.6V. Galvanostatic charge-discharge measurements were taken at different values of current densities. Figures 3.42-3.46 show the charge-discharge characteristics of samples at different values of current. Figure 3.47 shows the comparison of GO, PPy and 3PPyGO in galvanostatic charge-discharge performance. The curves of the three materials show that 3PPyGO nanocomposites have improved electrochemical performance as compared to PPy and GO. Also, it was observed that polypyrrole, compared to nanocomposites, showed fast discharge, low conductivity and low capacitance. The addition of GO to polypyrrole improved the electrochemical performance.

Discharging curves were used to calculate the specific capacitance of the electrodes. The following equation is used to calculate specific capacitance of the electrodes:

$$C_{sp} = \frac{I \times \Delta t}{\Delta V \times m}$$

where, m is the mass of the active materials, ΔV is the potential window, t is the discharge time and I is the discharge current. It is noted that the specific capacitance of the materials decreases with an increase in discharge currents, as seen in Figures 3.48-3.52. This could be due to insufficient Faradaic reaction and a higher potential drop at a higher discharge rate. Figure 3.53 shows the comparison of the galvanostatic charge-discharge performances of GO, PPy and 3PPyGO. As seen, the capacitance of 3PPyGO is twice that

of GO and PPy. A maximum specific capacitance of 190 F/g was observed for 3PPyGO sample, which is high compared to other nanocomposites, indicating the synergistic effect of GO in polypyrrole.

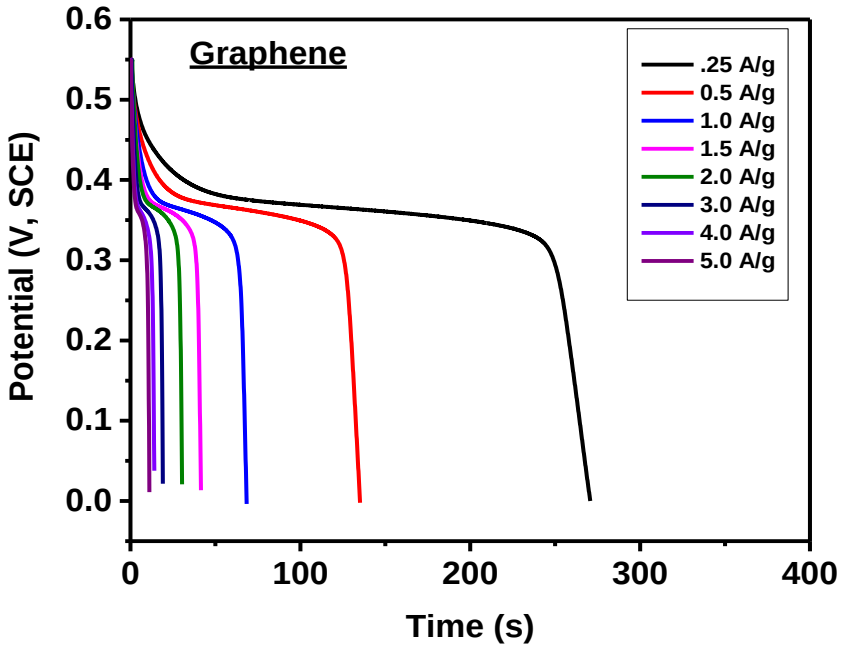

Figure 3.42: Galvanostatic charge-discharge characteristics of GO electrode at various applied currents in 3M KOH electrolyte.

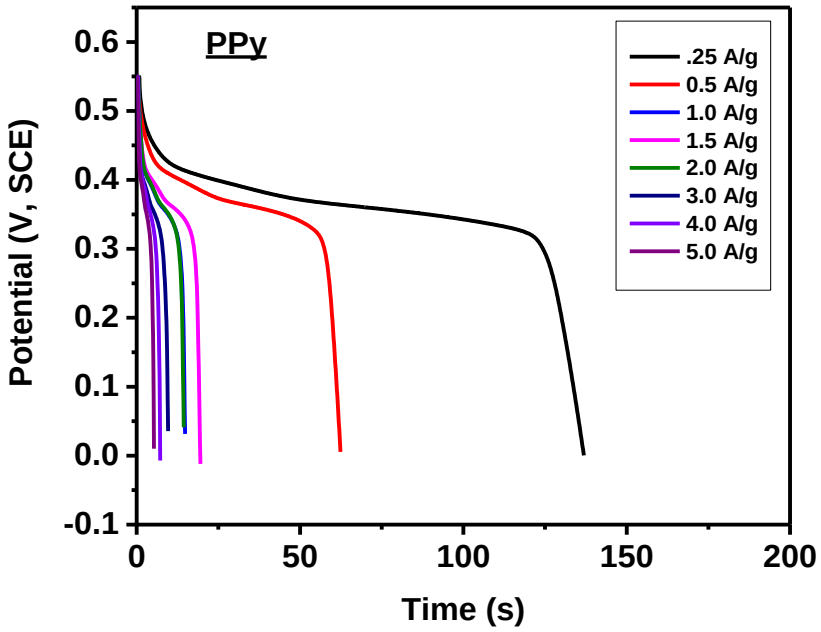

Figure 3.43: Galvanostatic charge-discharge characteristics of PPy electrode at various applied currents in 3M KOH electrolyte.

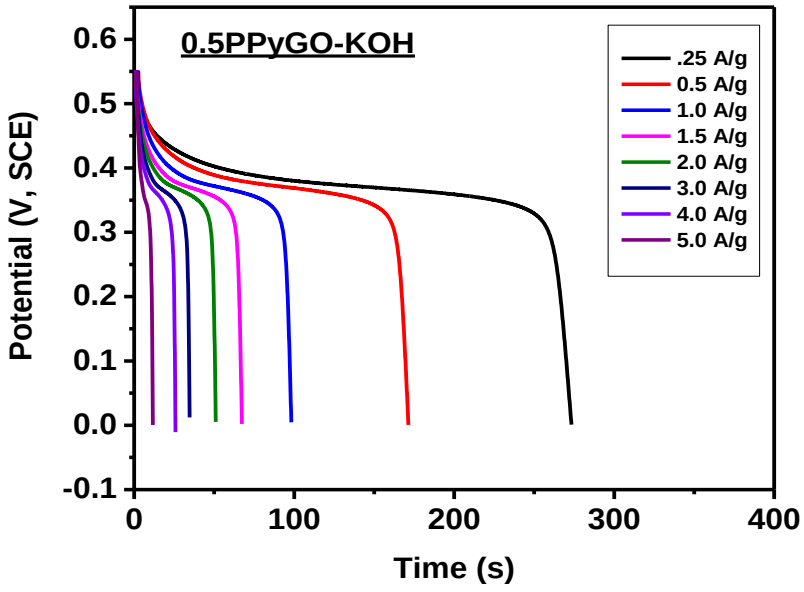

Figure 3.44: Galvanostatic charge-discharge characteristics of 0.5PPyGO electrode at various applied currents in 3M KOH electrolyte.

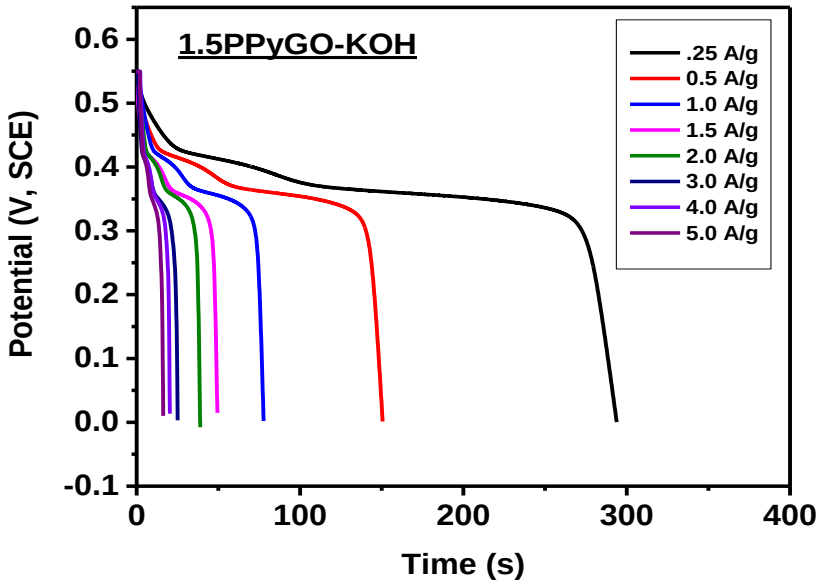

Figure 3.45: Galvanostatic charge-discharge characteristics of 1.5PPyGO electrode at various applied currents in 3M KOH electrolyte.

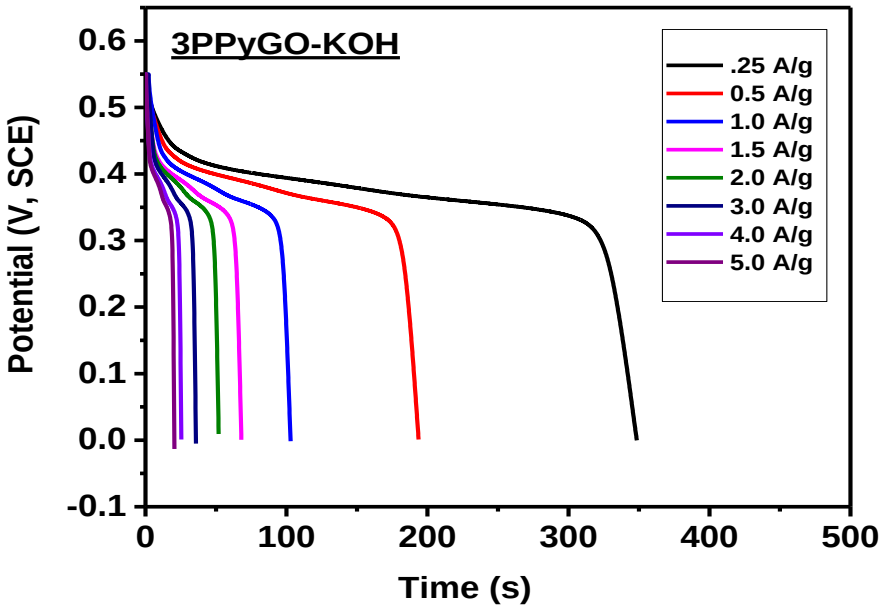

Figure 3.46: Galvanostatic charge-discharge characteristics of 3PPyGO electrode at various applied currents in 3M KOH electrolyte.

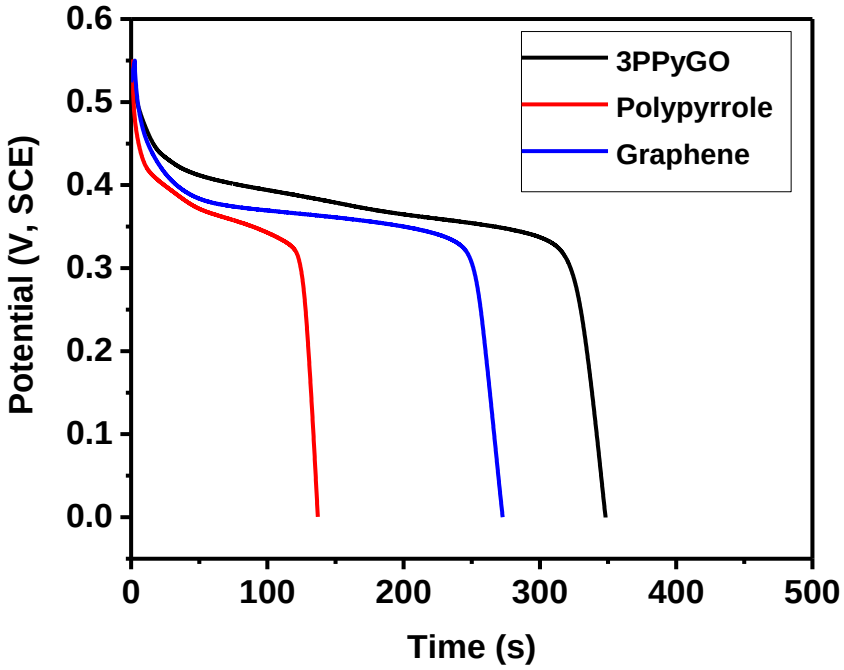

Figure 3.47: Comparison of GO, PPy and 3PPyGO in galvanostatic charge-discharge performance.

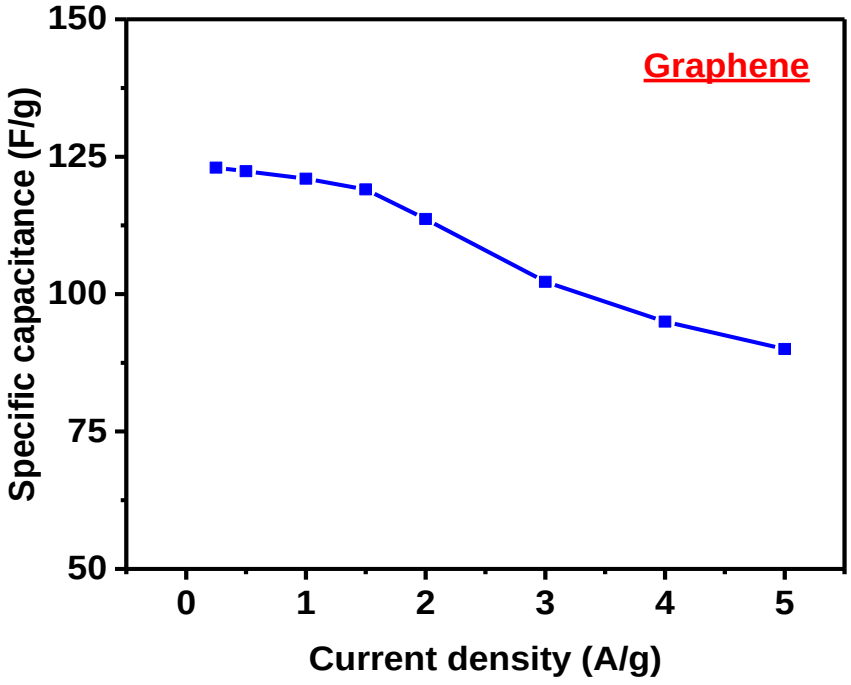

Figure 3.48: Specific capacitance as a function of current density for GO sample in 3 M KOH electrolyte.

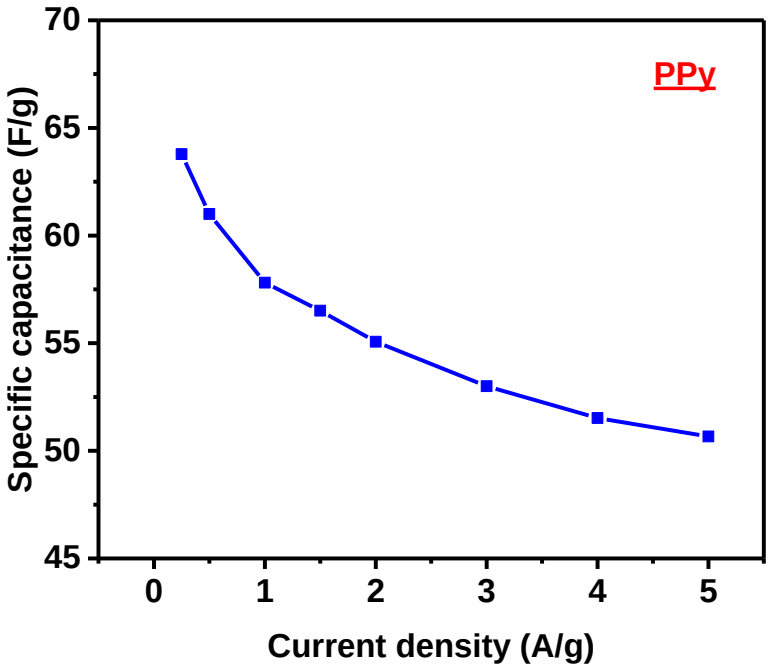

Figure 3.49: Specific capacitance as a function of current density for PPy sample in 3M KOH electrolyte.

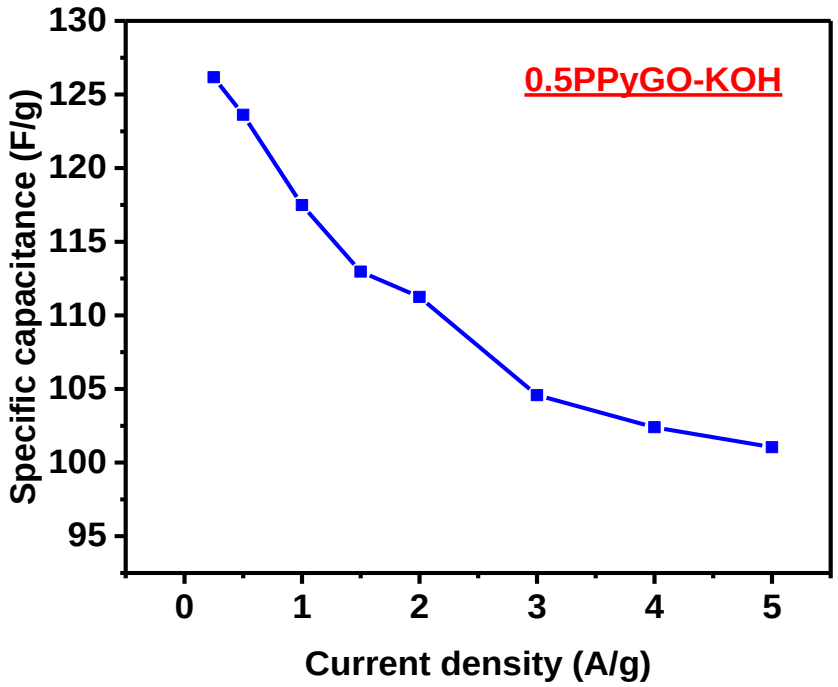

Figure 3.50: Specific capacitance as a function of current density for 0.5PPyGO sample in 3M KOH electrolyte.

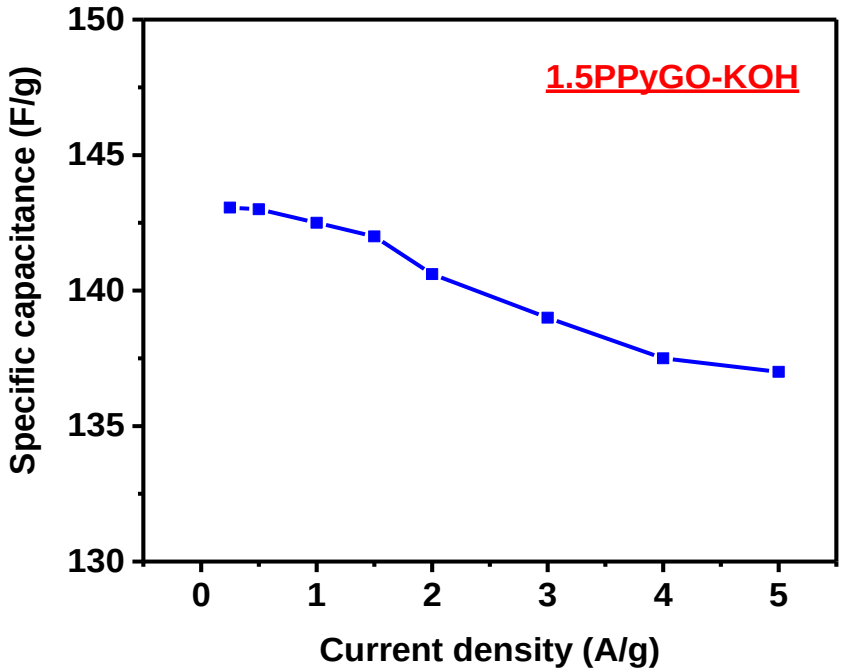

Figure 3.51: Specific capacitance as a function of current density for 1.5PPyGO sample in 3M KOH electrolyte.

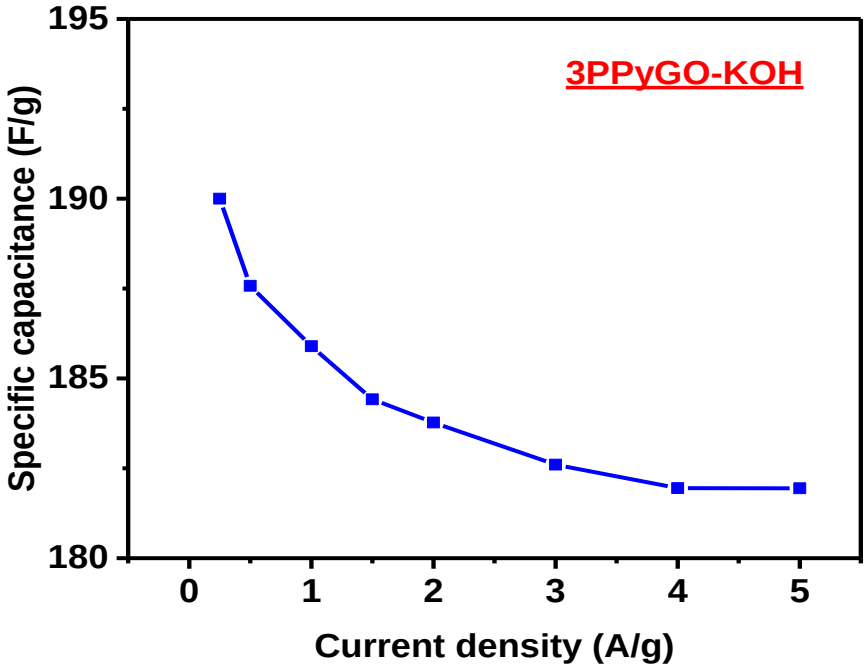

Figure 3.52: Specific capacitance as a function of current density for 3PPyGO sample in 3M KOH electrolyte.

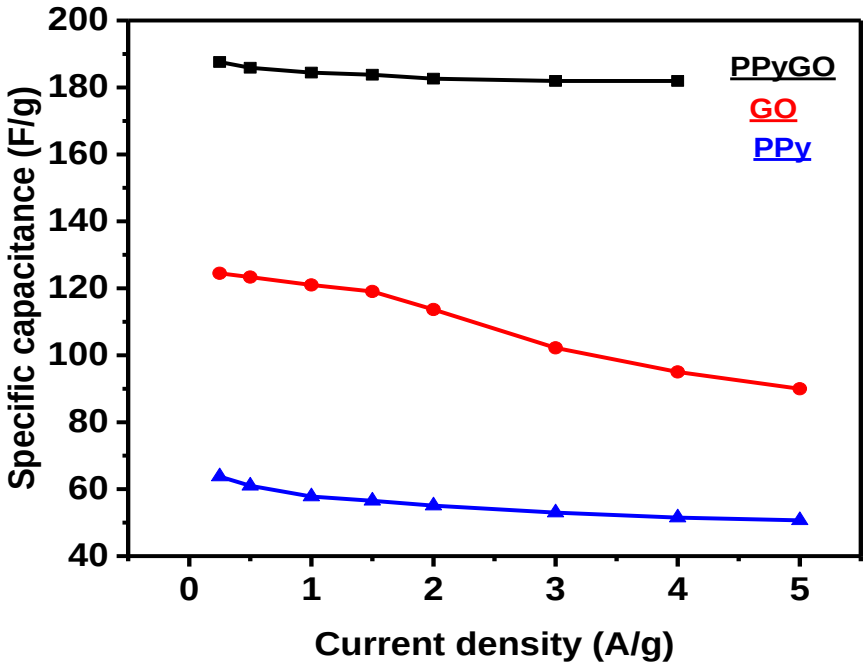

Figure 3.53: Comparison of GO, PPy and 3PPyGO in specific capacitance as a function of current density.

Table 3.2: Comparison of GO, PPy and PPyGO nanocomposites in specific capacitance as a function of current density.

Sample	specific capacitance Vs. scan rate
Polypyrrole	63 F/g
Graphene	124 F/g
0.5PPyGO	126 F/g
1.5PPyGO	143 F/g
3PPyGO	190 F/g

CHAPTER IV

CONCLUSION

Graphene nanoribbons were synthesized by unzipping the MWCNT. A facile chemical method was used to synthesize nanocomposites of PPy and GO. The synthesized materials were structurally characterized using XRD, SEM, Raman spectroscopy, FTIR, TGA, and BET. Using SEM, it was observed that the nanocomposites are made of nanoparticles of polypyrrole. A large number of pores were observed in the composites. PPYGO has a higher surface area than PPy which improves the charge storage capacity of the nanocomposites.

The TGA test conducted on the nanocomposite demonstrates a uniform weight loss as a function of temperature. Initial loss is related to the elimination of adsorbed water from the sample. The consistent dispersion of PPy nanoparticles on GO matrix is deduced from the similar TGA profiles. The electrochemical measurements showed the highest specific capacitance of 2,066 F/g for 3PPyGO, which was observed to decrease with increasing scan rates. The electrochemical properties were further analyzed using galvanostatic charge-discharge measurements. The specific capacitance of electrodes was observed to decrease with increasing current density. A maximum specific capacitance of 190 F/g was observed in 3M KOH solution for 3PPyGO sample.

The electrochemical results suggested that nanocomposites could be used as an electrode material for fabrication of high capacity supercapacitors. Finally, this study can be extended to the self-assembly of other conducting polymer and graphene nanoribbons through a simple route for various applications.

REFERENCES

1. Bakshi, A. K.; Bhalla, G. *J. Sci. Ind. Res.*, **2004**, *63*, 715-728.
2. Heeger, A. *Synth. Met.*, **2001**, *125*, 23-42.
3. Cheng, Y.; Yang,; S. H.; Hsu, C. *Chem. Rev*., **2009**, *109*, 5868-5923.
4. Jiles, D. *Introduction to the Electronic Properties of Materials*, Chapman & Hall: London, 1994.
5. Fan, L.-Z.; Maier, J. High-Performance Polypyrrole Electrode Materials for Redox Supercapacitors. *Electrochem. Commun.* **2006**, *8*,. 937-940.
6. An, H.; Wang, Y.; Wang, X.; Zheng, L.; Wang, X.; Yi, L.; Bai, L.; Zhang, X. Polypyrrole/Carbon Aerogel Composite Materials for Supercapacitor. *J. Power Sources*. **2010**,.*195*, 6964-6969.
7. Bibi, S.; Ullah, H.; Ahmad, S.; Shah, A.; Bilal, S.; Tahir, A.; Ayub, K. Molecular and Electronic Structure Elucidation of Polypyrrole Gas Sensors. .*J.Phys. Chem. C*. **2015**, *119*, 15994-16003.
8. Lee, J.; Kim, E.; Kim, D.; Park, J.; Hong, S. Nano-Storage Wires. *ACS Nano.* **2013**, *7*, 6906-6913.
9. Sultana, I.; Rahman, M.; Li, S.; Liu, H. Electrodeposited Polypyrrole (PPy)/para (Toluene Sulfonic Acid) (pTS) Free-Standing Film for Lithium Secondary Battery Application. *Electrochim. Acta*. **2012**, *60*, 20-205.
10. Biswas, S.; Drzal, L. Multilayered Nanoarchitecture of Graphene Nanosheets and Polypyrrole Nanowires for High Performance Supercapacitor Electrodes. *Chem. Mater.* **2010**, *22*, 5667-5671.

11. Letheby , H. On the Production of a Blue Substance by the Electrolysis of Sulphate of Anilene. *J. Chem. Soc.* **1862**, *15*, 161-163.
12. Shimano, J.Y.; MacDiarmid, A.G. Polyaniline a Dynamic Block Copolymer: Key to Attaining its Intrinsic Conductivity? *Synth. Met.* **2001**, *123*, 251-262.
13. Green, A.G.; Woodhead, A. E. Anilene-Black and Allied Compounds. Part II. *J. Chem. Soc., Trans.* **1912**, *101*,1117-1123.
14. Kim, B. C.; Ko, J. M.; Wallace, G. G. A Novel Capacitor Material Based on Nafion-doped polypyrrole. *J. Power Sources.* **2008**, *177*, 665–668.
15. Dietrich, M.; Heinze, J.; Heywang, G.; Jonas, F.; Schmidtberg, W. Polythiophenes, Process for their Preparation and their Use. U.S. Patent US4959430 A25, September 1990.
16. Wang, Y. Research Progress on a Novel Conductive Polymer–poly(3,4ethylenedioxythiophene) (PEDOT). *J. Phys.: Conf. Ser*., **2009**, *152*, 012023.
17. Novoselov, K. S.; Jiang, D.; Schedin, F.; Booth, T. J.; Khotkevich, V. V.; Morozov, S. V.; Geim, A. K. Proceedings of the National Academy of Sciences of the United States of America. **2005**, *102*, 10451.
18. Bolotin, K. I.; Ghahari, F.; Shulman, M. D.; Stormer, H. L.; Kim, P. Observation of the Fractional Quantum Hall Effect in Graphene. *Nature*. **2009,** *462*, 196.
19. Bae, S,; Kim, H.; Lee, Y.; Xu, X.; Park, J-S.; Zheng, Y.; Balakrishnan, J.; Lei, T.; Kim, H-R.; Song, Y. I.; Kim, Y-H.; Kim, K. S.; Özyilmaz, B.; Ahn, J-H.; Hong, B. H.; Iijima, S. Roll-to-Roll Production of 30-inch Graphene Films for Transparent Electrodes. *Nature Nanotech.* **2010**, *5*, 574-578.
20. May, J. W. Platinum Surface LEED Rings. *Surf Sci***. 1969**; *17*, 267.

21. Eizenberg, M,; Blakely, J. M. Carbon Monolayer Phase Condensation on Ni (111). *Surf. Sci.* **1979,** *82*, 228.

22. Somani, P. R.; Somani, S. P.; Umeno, M. Planer Nano-Graphenes from Camphor by CVD. *Chem. Phys. Lett.* **2006**, *430*, 56.

23. Varchon, F.; Feng, R.; Hass, J.; Li, X.; Nguyen, B. N.; Naud, C.; Mallet, P.; Veuillen, J.-Y.; Berger, C.; Conrad, E. H.; Magaud, L. Electronic Structure of Epitaxial Graphene Layers on SiC: Effect of the Substrate. *Phys. Rev. Lett*. **2007**, *99*, 126805.

24. Wang, J.; Xu, Y.; Zhu, J.; Ren, P. Electrochemical in Situ Polymerization of Reduced Graphene Oxide/Polypyrrole Composite with High Power Density. *J. of Power Sources*, **2012**, *208*, 138-143.

25. Fan, L.-Q.; Liu, G.-J.; Wu, J.-H.; Liu, L.; Lin, J.-M.; Wei, Y.-L. Asymmetric Supercapacitor Based on Graphene Oxide/Polypyrrole Composite and Activated Carbon Electrodes. *Electrochim. Acta.* **2014**, *137*, 26-33.

26. Kovtyukhova, N. I., Ollivier, P. J., Martin, B. R., Mallouk, T. E., Chizhik, S. A., Buzaneva, E. V.; Gorchinskiy, A. D. Layer-by-Layer Assembly of Ultrathin Composite Films from Micron-Sized Graphite Oxide Sheets and Polycations. *Chem. Mater*. **1999**, *11*, 771-778.

27. Jurewicz, K.; Delpeux, S.; Bertagna, V.; Beguin, F.; Frackowiak, E. Supercapacitors from Nanotubes/Polypyrrole Composites. *Chem. Phys. Lett*. **2001**, *347*, 36-40.

28. Schlange, A.; Dos Santos, A. R.; Kunz, U.; Turek, T. Continuous Preparation of Carbon-Nanotube-Supported Platinum Catalysts in a Flow Reactor Directly Heated by Electric Current. *Beilstein J. Org. Chem.* **2011**, *7*, 1412-1420.
29. Yang, Y.; Wang, C.; Yue, B.; Gambhir, S.; Too, C. O.; Wallace, G. G. Electrochemically Synthesized Polypyrrole/Graphene Composite Film for Lithium Batteries. *Adv. Energy Mater*. **2012**, *2*, 266-272.
30. Selvaraj, C.; Kumar, S.; Munichandraiah, N.; Scanlon, L. Reduced Graphene Oxide-polypyrrole Composite as a Catalyst for Oxygen Electrode of High Rate Rechargeable Li-O2 Cells. *J. Electrochem. Soc*. **2014**, *161*, A554-A560.
31. Gu, Z.; Li, C.; Wang, G.; Zhang, L.; Li, X.; Wang, W.; Jin, S. Synthesis and Characterization of Polypyrrole/Graphite Oxide Composite by In Situ Emulsion Polymerization. *J. Polym. Sci., Part B: Polym. Phys*. **2010** , *48*, 1329-1335.
32. Lingappan, N.; Gal, Y.-S.; Lim, K. T. Synthesis of Reduced Graphene Oxide/Polypyrrole Conductive Composites. *Mol. Cryst. Liq. Cryst*. **2013**, *585*, 60-66.
33. Fu, H.; Du, Z.-J.; Zou, W.; Li, H.-Q.; Zhang, C. Carbon Nanotube Reinforced Polypyrrole Nanowire Network as a High-Performance Supercapacitor Electrode. *J. Mater. Chem. A.* **2013**, *1*, 14943-14950.
34. Ye, S.; Feng, J. Self-Assembled Three-Dimensional Hierarchical Graphene/Polypyrrole Nanotube Hybrid Aerogel and its Application for Supercapacitors. *ACS Appl. Mater. Interfaces*. **2014**, *6*, 9671-9679.
35. Lim, Y. S.; Tan, Y. P.; Lim, H. N.; Tan, W. T.; Mahnaz, M.; Talib, Z. A.; Huang, N. M.; Kassim, A.; Yarmo, M. A. Polypyrrole/Graphene Composite Films

Synthesized via Potentiostatic Deposition. *J. of Appl. Polym. Sci.* **2013**, *128*, 224-229.